UNIVERSITY OF HELSINKI REPORT SERIES IN ASTRONOMY

No. 26

Rayleigh test and astronomical time point series: from Ancient Egyptian hemerologies to terrestrial impact craters

Sebastian Porceddu

ACADEMIC DISSERTATION

Department of Physics
Faculty of Science
University of Helsinki
Helsinki, Finland

To be presented, with the permission of the Faculty of Science of the University of Helsinki, for public criticism in Banquet Room, Unioninkatu 33 on 24th of November, 2020, at 12 o'clock.

Helsinki 2020

Cover picture: Perseus by Johannes Hevelius [@Public domain] and a periodogram of Cairo Calendar by author. Algol is shown as the evil eye of the Medusa.

ISSN 1799-3024 (print version)
ISBN 978-951-51-6648-7 (print version)
Helsinki 2020
Helsinki University Print (Unigrafia)

ISSN 1799-3032 (pdf version)
ISBN 978-951-51-6649-4 (pdf version)
http://ethesis.helsinki.fi/
Helsinki 2020
Electronic Publications @ University of Helsinki
(Helsingin yliopiston verkkojulkaisut)

Sebastian Porceddu: **Rayleigh test and astronomical time point series: from Ancient Egyptian hemerologies to terrestrial impact craters**, University of Helsinki, 2020, 48 p. + appendices, University of Helsinki Report Series in Astronomy, No. 26, ISSN 1799-3024 (print version), ISBN 978-951-51-6648-7 (print version), ISSN 1799-3032 (pdf version), ISBN 978-951-51-6649-4 (pdf version),

Abstract

Rayleigh test is a non-parametric method used to detect periodicity in time points. In this thesis the test is applied to Ancient Egyptian Calendars of Lucky and Unlucky Days and the terrestrial impact crater record. The Calendars of Lucky and Unlucky Days are ancient Egyptian texts where days or parts of days are given the evaluation 'good' or 'bad'. Mythological events pertaining to specific days are also described in the texts. These days and day parts were converted into time point data for analysis. Separate time point series were created for different selections of prognoses. Rayleigh test was used to search for periodicity in all these series of time points. Simulated time point data was also created in order to ascertain the statistical reliability in testing the real data. The simulations provided a "noise" periodogram which was used to normalize the periodogram of the real data. The significant discovered periods suggested influence from the synodic period of the Moon and the period of Algol's eclipses. These findings were analyzed in the context of Ancient Egyptian astronomy and mythology. In particular, the possibility of Ancient Egyptian observations of the variability of Algol required also a detailed astronomical and astrophysical discussion. Next the connection of these periods to selected words in the mythological text was explored. The time points related to chosen deities, nouns and locations were analyzed with the Rayleigh test. The results provided new insight into the arrangement of the texts in the calendars. Ten arguments supporting the evidence for ancient Egyptian observations of Algol were formulated on the basis of these results. As a separate experiment in Rayleigh test, this thesis also explains why it is currently not feasible to reliably discover periodicity in the terrestrial impact crater record. Samples of real impact crater data were used to create random crater data. This random data was tested assuming different ratios of periodic and aperiodic impacts, varying accuracy in determining crater age and the size of the data set.

Acknowledgements

This thesis would not have been possible without the kind help of various colleagues and collaborators. Foremost, I pay gratitude to the efforts of my supervisor Lauri Jetsu who introduced me to time series analysis methods and oversaw these adventures in science for more than a decade. Also I am very much indebted to two dearly missed professors: Tapio Markkanen who was paramount in supporting my interdisciplinary path and the first to notice that one of the many Cairo Calendar periods was close to Algol's period of variability; and Jaana Toivari-Viitala, our Egyptology teacher par excellence, who suggested the Calendar of Lucky and Unlucky Days as source material for time series analysis. Plenty of thanks go to various colleagues and professors who worked on these publications or supported us with comments and contributions: Patricia Berg, Rob Demarée, Heidi Jauhiainen, Perttu Kajatkari, Jyri Lehtinen, Joonas Lyytinen, Karri Muinonen and Heikki Oja. Last but not least, I am grateful to my wife Anja for being the sweetest companion one could wish for in a lifetime's quest for knowledge.

In memoriam
Tapio Markkanen (1942-2017)
Jaana Toivari-Viitala (1964-2017)

List of publications

Paper I: Porceddu, S., Jetsu, L., Markkanen, T. & Toivari-Viitala, J. 2008: Evidence of periodicity in ancient Egyptian calendars of lucky and unlucky days. Cambridge Archaeological Journal 18, 327-339

Paper II: Jetsu, L., Porceddu, S., Lyytinen, J., Kajatkari, P., Lehtinen, J., Markkanen, T. & Toivari-Viitala, J. 2013: Did the ancient Egyptians record the period of the eclipsing binary Algol - the Raging One? Astrophysical Journal 773, 1-14

Paper III: Jetsu, L. & Porceddu, S. 2015: Shifting milestones of natural sciences: the ancient Egyptian discovery of Algol's period confirmed. PLoS One 10, 12

Paper IV: Porceddu, S., Jetsu, L., Markkanen, T., Lyytinen, J., Kajatkari, P., Lehtinen, J. & Toivari-Viitala, J. 2018: Algol as Horus in the Cairo Calendar: the possible means and the motives of the observations. Open Astronomy 27, 232-263

Paper V: Lyytinen, J., Jetsu, L., Kajatkari, P. & Porceddu, S. 2009: Detection of real periodicity in the terrestrial impact crater record. Astronomy & Astrophysics 499, 601-613

Contents

Chapter 1

Introduction

The roots of astronomy lie deep in the dawn of mankind. To paraphrase the British astronomer J. Norman Lockyer, the earliest men regarded the Sun, the Moon and the stars with an attitude of worship [1]. The first applications of astronomy were calendars and astrology. These astronomical records from the past ages may still yield useful data. Some of them, however, may be obscured by the terminology of ancient scribes. This thesis aims to demonstrate the usefulness of searching for periodicity in time point series from archaic records.

The statistical Rayleigh test (also known as the R-test) was applied to search for periodicity in time point series based on the Ancient Egyptian Calendars of Lucky and Unlucky Days and the terrestrial impact crater record.

1.1 Ancient Egyptian astronomy

A central question of this thesis is: Could ancient Egyptians around 1224 BC have detected the brightness changes of the variable star Algol? The subject requires simultaneously considering its egyptological, astrophysical and astronomical implications. Thus I begin with an overview of ancient Egyptian astronomical practice.

Astronomical calendars were a part of ancient Egyptians' daily life. From the earliest times, a form of lunar timekeeping was used [2;3], with months and weeks based on the observed phases of the Moon, especially for timing religious festivals. The year was divided into three seasons of four months: "the flood season" Akhet, "the growing season" Peret and "the harvest season" Shemu. Because twelve lunar months do not comprise a solar year, a special "intercalary" month would have been used to synchronize the lunar and solar years.

For everyday business, a "civil" calendar was more practical. The civil year had 12 months, each of 30 days, with 5 "epagomenal" days added to the end of the year. The Egyptians might have noticed that a year with 365 days is one fourth of a day short of the solar year but there is no record of a leap year before the Roman times.

An ancient Egyptian sky map is depicted in the tomb of Senenmut ca. 1473 BC (Figs. 1.1, 1.2, 1.3) [5;6;7]. The map includes named stars or star groups belonging to the "decans", gods such as Isis and Osiris standing for Sirius and Orion and unspecified constellations such as Boat and Sheep. The planets Jupiter and Saturn appear in the painting as forms of the god Horus, whereas Venus is seen as god Bennu and Mercury as god Seth. Mars is also usually depicted as Horus but is not present in Senenmut's

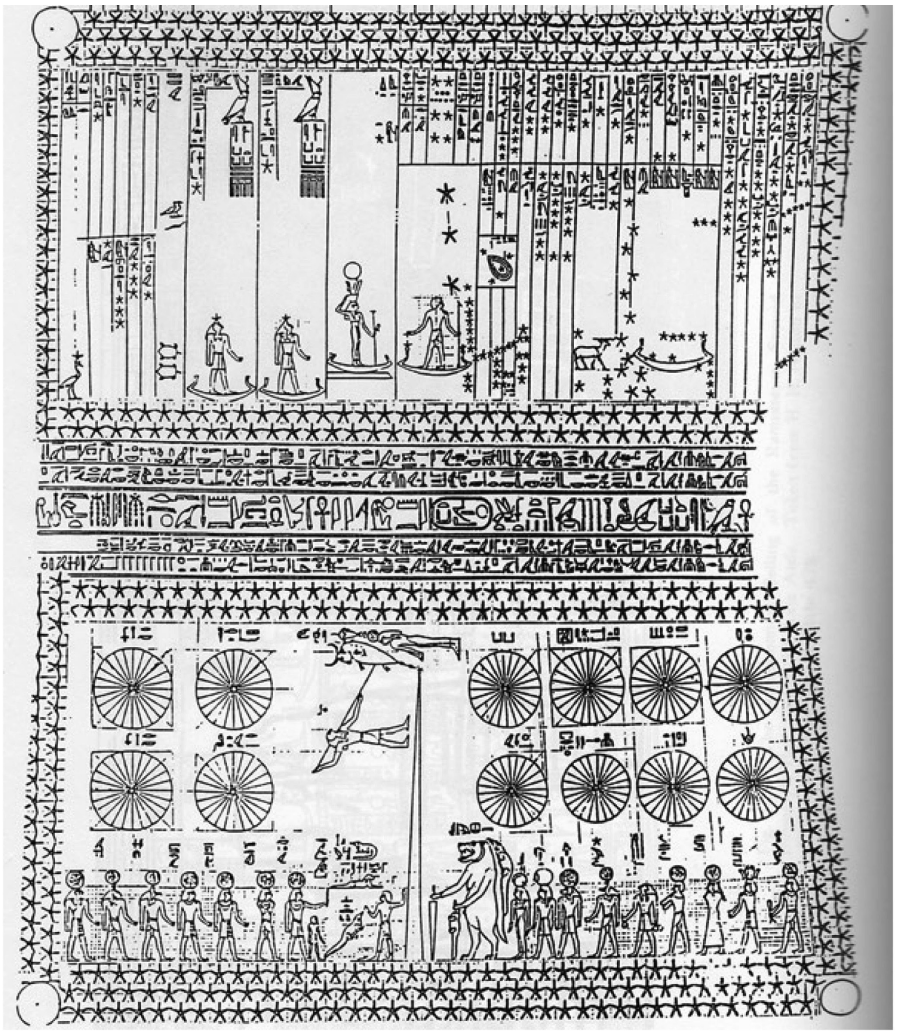

Figure 1.1: The ceiling of the tomb of Senenmut, 18th dynasty[4]. The figure is given to illustrate the standard form of depicting constellations and planets in Egypt, during the New Kingdom in particular. More details regarding this image are given in the text and Figs. 1.2 and 1.3.

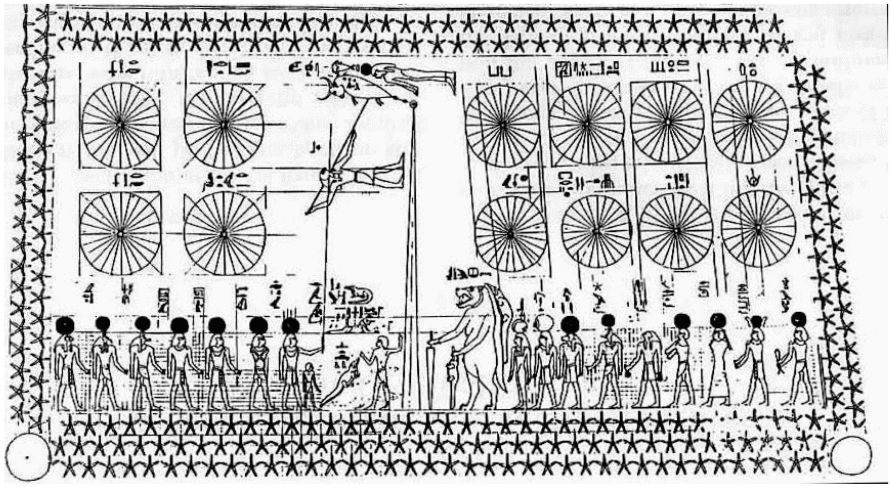

Figure 1.2: Detail from the northern half of the astronomical ceiling of Senenmut, 18th dynasty[4]. The constellation of the Ox, or the Foreleg of the Ox, is seen upper left. On the right side the Hippopotamus with the Crocodile on its back and its forelegs on the Mooring Post are depicted. On the left side the Man spears another Crocodile while above him are the small figures of the Bird and the Lion.

ceiling. Moon was traditionally connected with the "scribe of the Gods" Thoth (Fig. 3.1).

The northern side of the ceiling is occupied by "northern" constellations and gods with 12 wheels which are divided into 24 segments. The gods might have represented days. The wheels represent months and the segments are the hours of the day and the night combined. The Foreleg of the Ox, known to us as the Big Dipper, is a prominent one among the "northern" constellations. On its right side the Hippopotamus carries the Crocodile on its back and its forelegs rest on the Mooring Post. The Bird sits upon the Lion while below another Crocodile is being speared by the Man.

Inscriptions in the tombs of Seti I (ca. 1279 BC) and Ramses IV (ca. 1149 BC) contain excerpts from a text whose title was deciphered by Lieven[8] to be "The Fundamentals of the Course of the Stars". Papyrus Carlsberg I (ca. 100-200 AD) also contains a version of the text. It describes the journey of the Sun through the body of the sky goddess Nut (Fig. 7.1) into the underworld and using stars as a celestial clock.

The idea of a star clock dates back to at least the Old Kingdom (ca. 2686–2181 BC). The earliest known evidence is in the Pyramid Texts of the 24th century BC[3]. Actual representations of star clocks were found in coffins of the 22nd century BC. These are tables of 36 columns (one for each week of ten days) and 12 rows (one for each of the 12 night hours), naming the stars that divide the hours. If such a star, also called a decan, begins or ends the 12th hour of the night during a given week, it starts or ends the 11th hour of the next week. A week later, it signifies the 10th hour, and so on. According to "The Fundamentals of the Course of the Stars" any decan "works" for 120 days as its upper culmination is observed in the region of the meridian. For the next 90 days the decan is in the western hemisphere, before

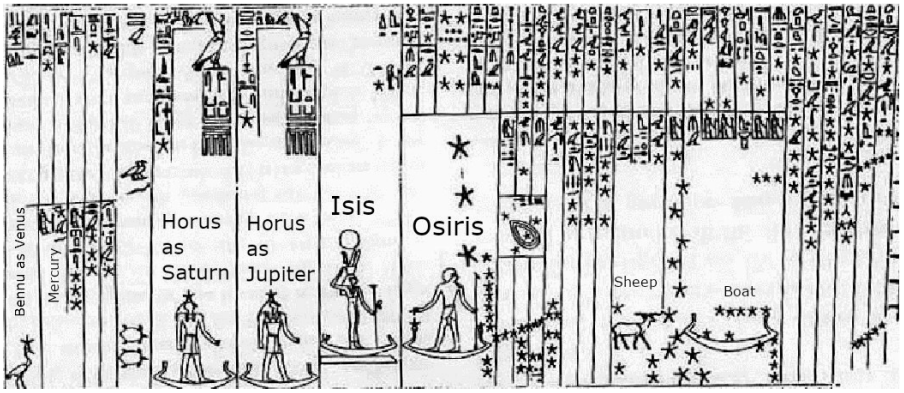

Figure 1.3: Detail from the southern half of the astronomical ceiling of Senenmut, 18th dynasty[4]. The main deities and constellations are named in the picture.

descending into the underworld for 70 days. After it rises heliacally it spends 80 days in the eastern hemisphere before returning to "work" upon the meridian.

A later star clock is known from the 12th century BC tombs of Ramses VI, Ramses VII and Ramses IX. It is a system of 13 rows of stars arranged into 24 columns. The first row gives the star that starts the first hour of the night. The rest of the rows give the stars that end the hours of the night. The stars are shown in positions around a humanoid figure: "upon the right shoulder", "upon the right ear", "upon the right eye", "opposite the heart", "upon the left eye", "upon the left ear" and "upon the left shoulder".

By the Late Period (712-323 BC) the Egyptian decans were amalgamated with the Babylonian zodiac[5;3]. The earlier decans eventually became obsolete, which is why most of the ancient Egyptian names for stars and constellations remain unidentified from the sky.

1.2 Impact craters

Next we will discuss the background for our studies of periodicity in impact cratering. The connection between our study of Ancient Egyptian astronomy and our study of impact craters across the globe is that Rayleigh test was utilized for both, showing the flexibility of this statistical method. In ancient times, men probably worshipped stones that had fallen from the sky, or considered them magical. Ceremonial objects have been found, such as a dagger blade from the tomb of Tutankhamun, that were manufactured from meteorite (*bi3 n pt*, "iron of the sky")[9]. Until the nineteenth century there was debate regarding the origin of such rocks. The Slovakian physicist Ernst Chladni proposed in 1794 that meteorites are of extraterrestrial origin. The theory slowly gained support when the stones obtained in the great meteor showers of Siena 1794, Yorkshire 1795, Benares 1798 and L'Aigle 1803 were analyzed chemically[10].

In the late 19th and early 20th centuries several scientists argued that craters were produced in impact events but the idea was not yet popular with geologists. After

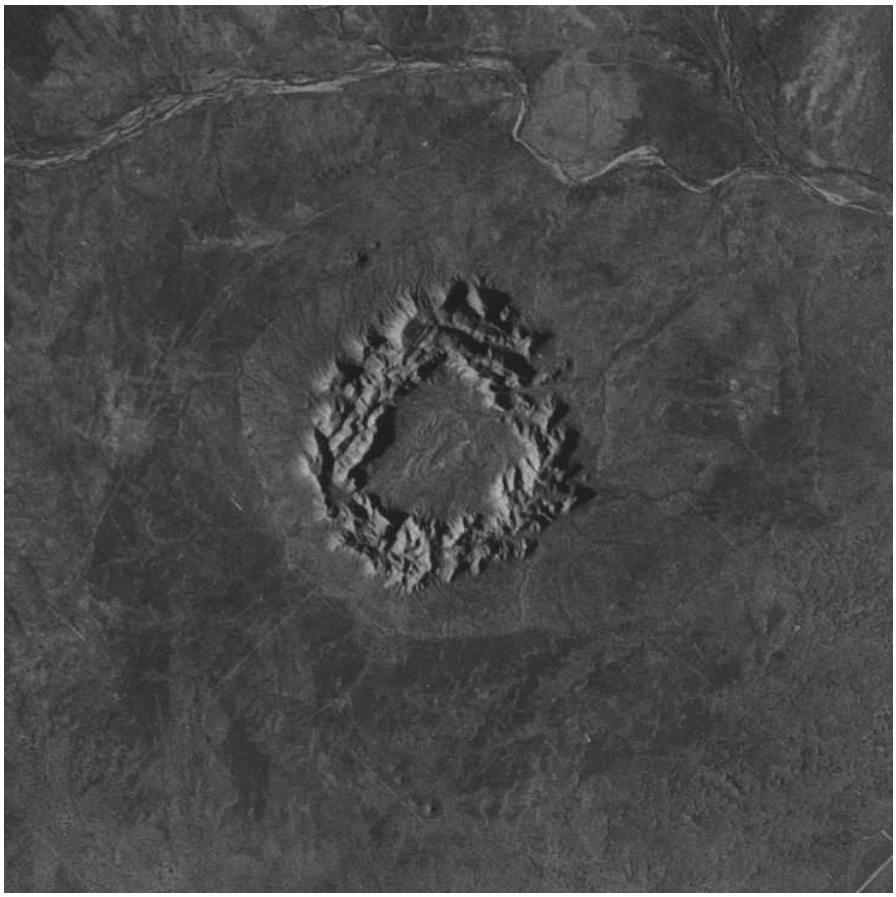

Figure 1.4: An impact crater example, Gosses Bluff[13].

the first earth-crossing asteroids were discovered in the 1930s, American meteoriticist Harvey Nininger published a study regarding the implications of asteroid impact on flora, fauna, the sea and the atmosphere[11]. Palaeontologist De Laubenfels proposed in 1956 that impacts might already have shaped terrestrial life in the past, while Opik in 1958 connected this with the boundaries between geological periods. However, until the research of Robert Dietz in the 1960's many of the impact craters were commonly considered cryptovolcanic[12].

Urey (1973) used the ages of tektites as evidence that geological periods have been terminated by asteroid or comet impacts with Earth[14]. Since then at least the major extinction event at the Cretaceous-Paleogene boundary 65 million years ago has been reliably connected with a cosmic impact, even though other phenomena alongside the impact contributed to the extinction[15]. However, tracing impact history is difficult because sedimentation, erosion and plate tectonics gradually hide older craters. So far about 190 terrestrial impact structures have been identified (Fig. 1.4). A recent study compared the cratering rates of Moon and Earth, concluding that hundreds of

smaller craters ($\varnothing < 6$km) are still undiscovered[16]. Also the record of very old craters ($t > 600$Mya) is still rather limited.

Another matter of dispute is the periodicity of cosmic impacts. Impacting objects can be NEAs (near-Earth asteroids) or NECs (near-Earth comets) from the Oort cloud. Most craters are due to NEAs, but craters caused by NECs are more prominent because impacting comets tend to have a larger impact velocity and size, and thus these impacts release more energy[17]. Several papers have argued for the presence of a periodic component 26 Myr to 36 Myr in the crater data. The 26 Myr periodicity was first suggested in the mass extinctions of species by Raup & Sepkoski in 1984[18] who analyzed fossil records. The connection with impact craters was elaborated in five articles of Nature issue 308[19;20;21;22;23]. The 26 Myr periodicity was explained with the oscillation of Solar System in the plane of the Galaxy, or with a solar companion star initiating comet showers from the Oort cloud. Periodic passage through the spiral arms of the galaxy has been suggested to induce heightened exposure to impacts, cosmic rays and supernovae[24;18]. More recently, Rohde & Müller[25] and Melott & Bambach[26] found a 62 Myr period in the extinctions of marine species, while Rampino & Caldeira[27] argued again for a 26 Myr periodicity in crater ages. Over the years many studies have argued for and against periodicity[28;29;30;31;32;33]. For example, Meier & Holm-Almwark showed that the 26 Myr periodicity disappears when more precise crater ages[28] are used, because periodicity is caused by "clusters" of contemporary craters. These may have been caused by a larger object breaking into fragments that impact the Earth at the same time. Our Paper V addresses this question: If some Earth impacts are periodic (for example of cometary origin), can such periodicity be detected from the available data?

Chapter 2

Rayleigh test

In the papers included in this thesis, the R-test (Rayleigh test) is applied to search for periodicity in time point series.

Periodicity in a series of time points $t_1 \leq t_2 \leq ... \leq t_n$, where n is the number of the time points, can be analyzed with parametric or non-parametric methods. In each paper of this thesis, the non-parametric Rayleigh test is applied to search for periodicity in time points. No graphical model is assumed for these data. As there is no model, the method is called non-parametric. If the method relies on a model and the model has parameters, the method is parametric. Instead, in Rayleigh test the hypothesis H_0 formulated in Ch. 2.1 is tested.

The Rayleigh test[35] has previously been utilized to test such hypotheses in at least chemistry, biology, geology, and astronomy. It has proved effective in searching for periods and quasi-periods in X-ray and γ-ray data, for example sunspots and the emissions from Jupiter's aurora[36;37;38]. It is historically based on a solution for Pearson's random walk problem[39], which was formulated as:

> *A man starts from a point 0 and walks l yards in a straight line; he then turns through any angle whatever and walks another l yards in a second straight line. He repeats this process n times. I require the probability (Q) that after these n stretches he is at a distance between r and r + dr from his starting point 0.*

Its first practical application was as a description of polymer configurations.[40] R-test means testing a hypothesis: a "walk" is random. If the "walk" has a specific direction the random hypothesis is rejected. The test gives the probability for a signal being present in a sample of circular data (i.e. data measured in angles or directions).

A time point series t_i becomes such circular or directional data, if the time points are transformed into unit vectors pointing to a direction calculated according to the chosen period P or frequency $f = P^{-1}$. The directions of these unit vectors are the phase angles $\Theta = 2\pi(t - t_0)/P$. A pair of time points separated by an integer multiple of the period P have identical phase angles Θ when transformed to circular data.

Let us formulate the R-test for n time points t_i with an arbitrary period P and frequency $f = P^{-1}$.

The phases ϕ_i of a time point t_i with period P and frequency f and the corresponding phase angles θ_i are calculated as follows:

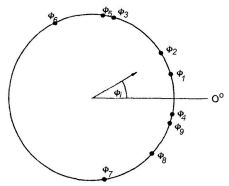

Figure 2.1: An example of time points t_i transformed into phases ϕ_i using Eq. 2.1.

$$\theta_i = 2\pi\phi_i = 2\pi \times \mathrm{frac}[(t_i - t_0)P^{-1}], \tag{2.1}$$

where t_0 is the zero epoch and $\mathrm{frac}(x)$ means the fractional part of x, i.e. the excess beyond the number's integer part (e.g. $\mathrm{frac}[1.23] = 0.23$).

The above equation gives the phase ϕ_i of the time point t_i with the period P, where $0 \leq \phi_i < 1$, and the phase angle θ_i, where $0 \leq \theta_i < 2\pi$. The transformation of time point to phase angle is graphically shown in Fig. 2.1.

The Rayleigh test statistic z is the vector sum of the unit vectors $r_i = [\cos\theta_i, \sin\theta_i]$.

$$z = n^{-1}[(\sum \cos\theta_i)^2 + (\sum \sin\theta_i)^2] = |R|^2/n. \tag{2.2}$$

Higher value of the test statistic means a higher probability that the data is not random. The vector $R = \sum_{i=1}^{n} r_i$ points to the direction $\theta_R = \arctan(R_y/R_x)$, where $R_x = \sum_{i=1}^{n} \cos\theta_i$ and $R_y = \sum_{i=1}^{n} \sin\theta_i$.

Note that the periodogram of discrete Fourier transform[41] or the convolution of true Fourier transform with a spectral window[42] with constant signal, i.e. without a scaling function, is equal to the Rayleigh test statistic.

The probability density function for the standard Rayleigh test statistic z is

$$f(z) = e^{-z}. \tag{2.3}$$

Note that the symbol f in this case does not denote frequency but the probability of random variable reaching the value. In this introduction I have chosen to utilize f for both meanings to maintain consistency and easy comparison with the source material. Its integral, the cumulative distribution function is

$$F(z) = 1 - e^{-z}. \tag{2.4}$$

The value $F(z_0)$ of the cumulative distribution function is the probability for the test statistic z being lower or equal to the value z_0.

$$P(z \leq z_0) = F(z_0) = 1 - e^{-z_0}. \tag{2.5}$$

The probability for the complementary event $z > z_0$ is

$$P(z > z_0) = 1 - F(z_0) = e^{-z_0} \tag{2.6}$$

Note that the last equation brings us back to the original problem of random walk: *Pearson's question: I require the probability (Q) that after these n stretches he is at a distance between r and r + dr from his starting point 0.*
Rayleigh's answer: If n be very great, the probability sought is $\frac{2}{n}e^{-r^2/n}rdr$.[43]

For large n, the result is consistent with Eq. 2.6 as an integral of Rayleigh's function from R to ∞.

$$Q = e^{-z} = e^{-(R^2/n)} \tag{2.7}$$

2.1 Testing an arbitrary frequency

R-test is performed to check if the "random walk" hypothesis is true, i.e. whether the data has a random distribution or not. The structure of the test is:

1: The null hypothesis (H_0) is made:
"The chosen time points t_i transformed to phases ϕ_i with an arbitrary frequency f are randomly distributed between [0,1]."

2: The preassigned significance level γ for rejecting H_0 is fixed. It is the probability for falsely rejecting H_0 when it is true.

3: The test statistic z_0 for the time point series $t_i, ..., t_n$ is calculated with the chosen frequency f.

4: The critical level $Q = P(z \geq z_0) = e^{-z_0}$ is calculated.

5: If $Q < \gamma$, the null hypothesis H_0 is rejected. If $Q \geq \gamma$, the null hypothesis H_0 is not rejected.

2.2 Testing several independent frequencies

The statistical test for one ($m = 1$) arbitrary frequency is described above. In practice we want to test many independent frequencies in a chosen interval $[f_{\min}, f_{\max}]$.

The distance between independent frequencies f_0 means that the $z(f)$ values do not correlate with $z(f + f_0)$. This requires that the phase difference of the first and last time points t_1 and t_n in the data with length ΔT is one full cycle. Thus, the distance between independent frequencies is

$$f_0 = \frac{1}{t_n - t_1} = \frac{1}{\Delta T}.$$

The choice of minimum and maximum frequency is arbitrary within the boundary conditions established by data spacing and data length:

$$f_{\min} = \frac{1}{P_{\max}} = \frac{1}{\Delta T} f_{\max} = \frac{1}{P_{\min}} = \frac{n}{\Delta T}$$

The periodogram $z(f)$ (Fig. 2.2) is then obtained by calculating the test statistic z of every independent frequency in the tested interval $[f_{\min}, f_{\max}]$. The number of tested independent frequencies is a ceiling function that produces an integer:

$$m = \lceil \frac{f_{\max} - f_{\min}}{f_0} \rceil \tag{2.8}$$

Testing many independent frequencies requires recalculating the probability for the test statistic z exceeding the limit z_0. The probability for $z > z_0$ in a single test ($m = 1$) was given in Eq. 2.6. The probability for the complementary event $z \leq z_0$ was given in Eq. 2.5.

It follows that the probability for z not exceeding z_0 even once when testing m independent frequencies f is

$$P(z \leq z_0) = (1 - e^{-z_0})^m.$$

The probability for z being at least once higher than z_0 in m tests is equal to the probability of the complementary event of the above

$$P(z > z_0) = 1 - (1 - e^{-z_0})^m \tag{2.9}$$

This probability $Q = P(z > z_0)$ is the critical level. If $Q < \gamma$ in any of the m statistically independent tests, the null hypothesis H_0 is rejected. To be precise, the significance estimates are valid only for the highest peak. Considering the complementary idea, the probability for more than one peak higher than z_0 in m tests is actually lower. Thus, in this case, significance may be underestimated.

The accuracy in the position of the peak can be improved by overfilling, i.e. dividing the frequency step f_0 by a factor G[33]. Overfilling within an interval $\pm f_0/2$ does not have any consequences for the statistics, because these tests are not independent.

2.3 Bootstrap error estimates

The standard error σ_f of the best frequency f_{best} determined with the R-test can be estimated with different approaches. In all articles presented here the bootstrap[44] is used to estimate σ_f. In this method, we randomly sample $\overline{t}^*$ from the original time series $\overline{t} = [t_1, ..., t_n]$. Any time point in $\overline{t}$ may be included into $\overline{t}^*$ several times or not at all. The number of samples $\overline{t}^*_1, ..., \overline{t}^*_S$ created from the data is S. For each sample, the Rayleigh test is performed for the frequency interval $[f_{\text{best}} - f_0/2, f_{\text{best}} + f_0/2]$. This gives the best frequency $f_{\text{best},j} (j = 1, ..., S)$ for each particular $\overline{t}^*_j$ sample (Fig. 2.3). After the best frequency of all S random samples has been calculated, the standard deviation of these S best frequencies $f_{\text{best},j}$ gives σ_f.

$$\sigma_f = \sqrt{\frac{1}{S-1}} \sum_{j=1}^{S} (f_{\text{best},j} - \langle f_{\text{best}} \rangle), \tag{2.10}$$

$$\langle f_{\text{best}} \rangle = (1/S) \sum_{j=1}^{S} f_{\text{best},j}$$

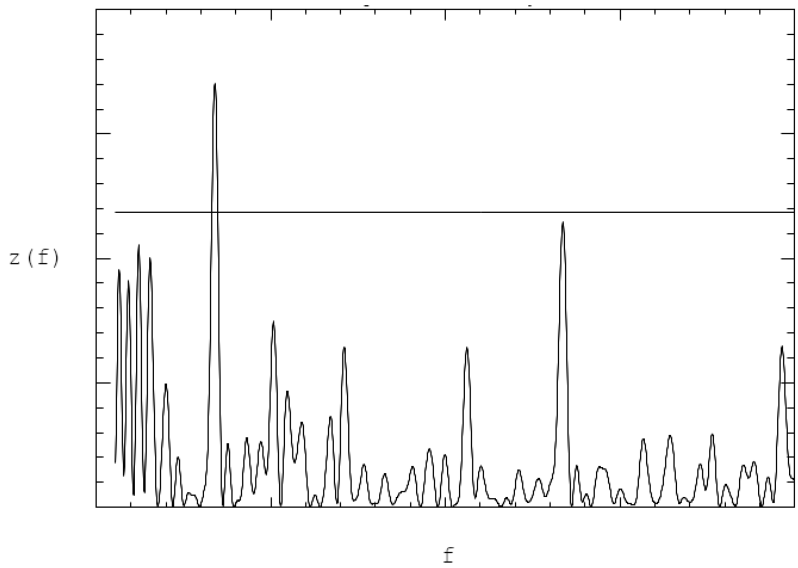

Figure 2.2: An example of periodogram z_f produced by calculating the test statistic z of every independent frequency in the interval $[f_{\min} = 0.0, f_{\max} = 0.2]$ with overfilling factor $G = 20$. The line represents the z_0 for $Q = P(z > z_0) < \gamma$, where $\gamma = 0.01$. In other words, 1% of random samples will reach this level. Because at least one $z(f)$ value is higher than the critical level, the null hypothesis H_0 is rejected.

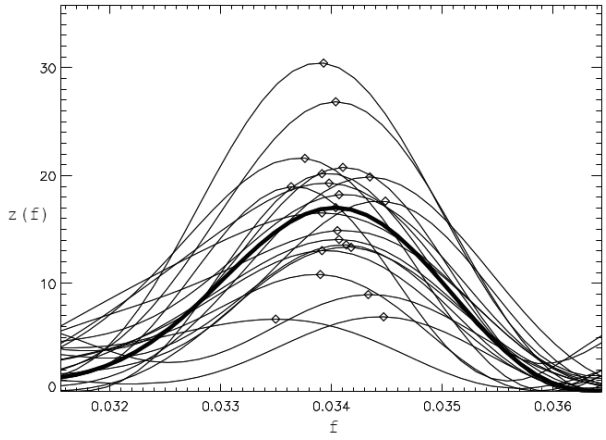

Figure 2.3: An example of using bootstrap to estimate standard error σ_f for $f = 0.034$. The periodogram calculated from the original data with overfilling factor $G = 20$ is denoted by the thick line. The periodograms of samples $\overline{t}^*$ are denoted by the narrow lines. The diamonds mark the best frequency f_{best} for each sample. The standard deviation of these best frequencies gives $\sigma_f = 0.003$.

2.4 Spurious periods

Let us assume that besides the real period P, an interfering period P_0 is present in the data. Consequently, time points separated by multiples of P_0 may cause a spurious period P' appear in the periodogram. This occurs because for a time point $t_i = t_0 + k_2 P_0$, where $k_2 = 1, 2, ...$, the phases are the same for the real period P and for the spurious period P':

$$\phi_i = \mathrm{frac}[(t_i - t_0)/P] = \mathrm{frac}[k_2 P_0/P]$$
$$\phi'_i = \mathrm{frac}[(t_i - t_0)/P'] = \mathrm{frac}[k_2 P_0/P'].$$

Relation $\phi_i = \phi'_i$ is fulfilled, if $k_1 = \pm 1, \pm 2, ...$ and

$$\mathrm{frac}[k_2 P_0/P] = \mathrm{frac}[k_2 P_0/P']$$
$$\Leftrightarrow k_2 P_0/P = k_2 P_0/P' + k_1.$$

The phases are equal, because their differences are full cycles $k_1 = \pm 1, \pm 2, ...$ Hence, spurious periods induced by the interference of P with P_0 can be predicted from

$$P' = [P^{-1} + k_1 (k_2 P_0)^{-1}]^{-1}. \tag{2.11}$$

Negative values of k_1 result in phase difference $-1, -2, -3, ...$, producing "mirrored" phase distributions for P and P'. It is not easy to recognize all spurious periods with this simple equation because the combinations of the variables are endless. However, at least some spurious periods can be noticed with the help of these relations.

For example, in testing for the periodicity of prognoses in the Cairo Calendar (Paper II) the period $1^{\mathrm{d}}.54$ was found to be a spurious period predicted by Eq. 2.11 where $P_1 = 2.85$ (the proposed period of Algol), $P_2 = 1.0$ (an artifact of the regular spacing of the time points), $k_1 = -1$ and $k_2 = 1$.

Chapter 3

Periodicity of prognoses in the Cairo Calendar

Paper I was the beginning of a veritable adventure: this study regarding the Ancient Egyptian calendars of lucky and unlucky days would spawn three more papers (Papers II-IV). It started with the idea of using the R-test to determine if the so-called prognoses ('good' and 'bad' assigned to parts of days) were distributed randomly or periodically within the year.

Calendars of lucky and unlucky days, also known as hemerologies, are ancient Egyptian texts that describe prognoses 'good' (*nfr*) and 'bad' (*ḥȝ*) with related suggestions and prohibitions for the days of the year. In Paper I, the prognoses from papyrus Cairo 86637, papyrus Sallier IV and papyrus BM 10474 were tested for periodicity. Previous studies[45;46;47;48] on hemerologies had already suggested that some astronomical events influenced the prognoses. However, the only clearly visible periodicity was that the 'good' prognosis is repeated for every 1st day of the month and 'bad' prognosis for every 20th day of the month. Mythological events relating to specific dates are also described. In all the source texts studied here, three separate prognoses were assigned for each day - usually taken as one for the morning, one for the mid-day and one for the evening. An example is shown in Table 3.1.

The prognoses from the three mentioned sources were tabulated according to Leitz[47]. Any unclear or incomplete prognoses were ignored. In Paper I we created three time points for each day: one for the morning, second for the mid-day and a third for the evening. It is not known for certain if the third prognosis was supposed to include also the nighttime, but dividing the daytime into three equal parts was considered sufficient. We proved that the day division is irrelevant regarding the main results.

Table 3.1: An example of the prognoses in Cairo Calendar. Days I Akhet 1-10.

Day	First part of day (morning)	Second part of day (mid-day)	Third part of day (evening / night)
I Akhet 1	good	good	good
I Akhet 2	good	good	good
I Akhet 3	good	good	bad
I Akhet 4	good	good	bad
I Akhet 5	good	good	good
I Akhet 6	bad	bad	good
I Akhet 7	good	good	good
I Akhet 8	good	good	bad
I Akhet 9	good	good	good
I Akhet 10	good	good	good

The declination δ of the sun was obtained with the day number N counted from the Gregorian New Year's day:

$$\delta = -23.45^\circ \cos([360/365]N + 10)$$

The Egyptian New Year was assumed to occur at $N = 187$. This epoch N was actually misread from Leitz[47] who used $N = 188$ as kindly later pointed out by Rolf Krauss. Luckily, this mishap did not have any consequences for the results, which we showed in Paper II to be independent of the concordance N.

The integer part of each time point was the day number, counted from the Egyptian New Year. The day number N_E was obtained from the month M and day D with the equation

$$N_E = 30(M-1) + D. \tag{3.1}$$

At the intermediate latitude of Egypt $\phi = 26^\circ 45\,\mathrm{min}$ the declination δ is:

$$cosH = \pm \tan\phi \tan\delta,$$

where + is for sunset and − for sunrise.

The length of the Egyptian daytime l_d was calculated from the hour angle of sunset and sunrise H, also known as the half day arc:

$$l_d = 2 \mid H \mid$$

The decimal parts for the three time points of the day were $l_d/(6 * 24\mathrm{h})$, $3 * l_d/(6 * 24\mathrm{h})$ and $5 * l_d/(6 * 24\mathrm{h})$.

Separate time point series were created from the prognoses given by papyri Cairo 86637, BM 10474 and Sallier IV. Time points were selected according to the occurrence of a prognosis combination (e.g. GGG, SSS, GGS) or the occurrence of a single prognosis (G or S) in a specific day part or any day part. GGG and SSS were the most common by far. Some rarely occurring combinations such as SGS and GSG did not yield enough time points for this study. For prognosis combinations, thirteen time point series were created. For individual prognoses, 24 time point series were created.

We did not analyze the prognoses as binary data (e.g. G represented by 1 and S represented by 0) but independently because wanted to avoid inducing noise from the S periods to G periodogram, and vice versa. Analysis of the prognoses as binary data remains a possible future experiment.

3.1 First evidence: the unmodified R-test

The tested period interval was $1^d.5 \leq P \leq 180^d$, and we used the preassigned significance level $\gamma = 0.01$ for rejecting H_0 (Fig. 3.2).

The null hypothesis H_0 was rejected in 11 cases. In these cases, we also calculated the error σ_P of the significant periods using the bootstrap method (see Ch. I, Eq. 2.10).

The best period in most of the time point series was $7^{\mathrm{d}}.5$. It was significant in series 32-37 and it reached the highest significance (i.e. lowest critical level) found in any of the series: $Q = 4.792 \times 10^{-7}$ in series 36. It was accepted as a real period in

Figure 3.1: Thoth, the patron of science and scribal profession, was also a lunar god. It has been suggested that an intercalary month named after Thoth was used to synchronize the lunar and solar calendars[49]. Drawing courtesy of Anja Isoaho.

Paper I and proposed as evidence for a division of the month into four "weeks". This interpretation was revised in Paper II.

Another prominent period was the period 30^{d}. It was the best period in series 32 and 35. It was noted that the mean length of the synodic month ($29^{\mathrm{d}}.531$) is within he error margin of $P_{\mathrm{best},1} = 29.39 \pm 0.24$ (series 32). The period of the Moon was evidence of an underlying lunar calendar.

The period $2^{\mathrm{d}}.4$ was the best period in series 37, the period $3^{\mathrm{d}}.16$ was the third best period in series 37 and the period $2^{\mathrm{d}}.85$ was the third best period in series 32. It was tentatively proposed that this 2.85 days period may be connected to the variable star Algol, whose brightness changes occur today in a $2^{\mathrm{d}}.867$ cycle.

3.2 Rising of Algol: the modified R-test

In Paper I, we used some assumptions in creating the time points for the prognoses. For example, we assumed that the time point for the third part of the day represented evening, even though it might have been meant to include the entire nighttime[47]. For Paper II, we created additional time point series Fig. 3.3 where the third time point of the day was

$$t_3(N_E) = (N_E - 1) + 1/2 + (1/2)[l_D(N_G)/24] \tag{3.2}$$

Another assumption concerned the concordance between the Egyptian (N_E) and Gregorian (N_G) days, so we tested time point series with $N_0 = 62$, $N_0 = 187$ and $N_0 = 307$. We also tested eliminating the day 1 of each month (which is always "GGG") and the day 20 of each month (which is always "SSS"). All these variations resulted in 24 time point series for the prognoses of papyrus Cairo 86637, abbr. CC. Out of the original source papyri, only CC was tested. Individual prognoses G or S, not prognosis combinations such as GGG or SSS, were used to create the time point series. The tested period interval in Paper II was $1^d.5 \leq P \leq 90^d$. Due to the

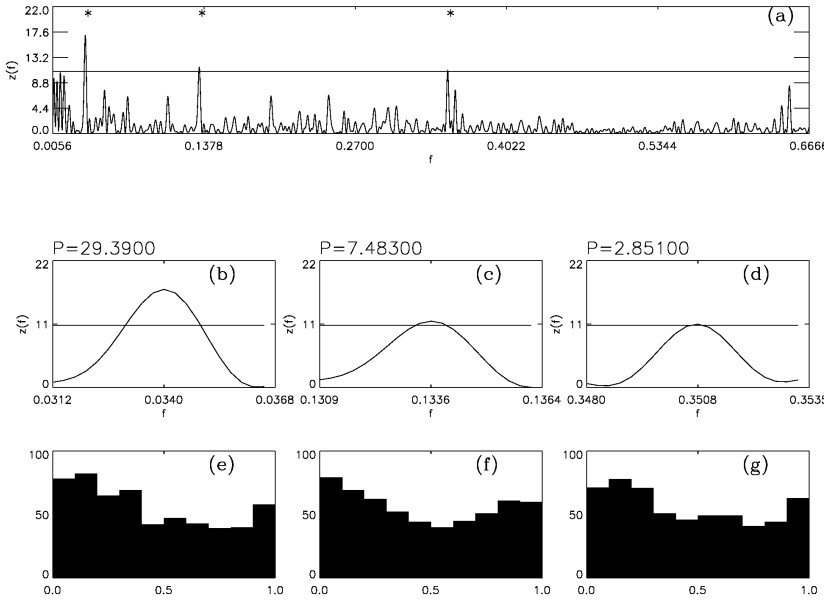

Figure 3.2: An example of the results of Paper I. (a) The periodogram of time series 32 with the three best periods marked. The horizontal line represents the critical level. Note the noise at short frequencies due to unreliable statistics when the tested period approaches the length of the data. This naturally vanished with the normalization applied in Paper II.(b-d) show a magnification of the periodogram in the vicinity of the three best periods. (e-g) show the phase distributions of time points for the three best periods.

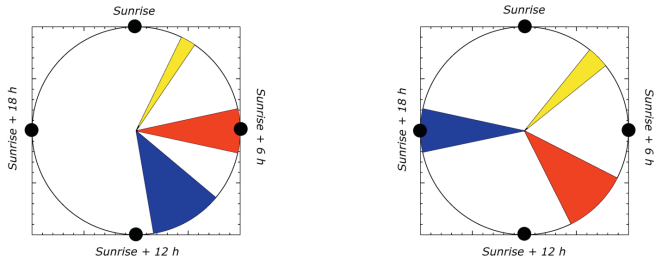

Figure 3.3: This graph shows the seasonal fluctuation in the assignment of time points for the first, second and third part of the day. The left circle shows time points created assuming the third part of the day in the Cairo Calendar refers to evening. The right circle shows time points created assuming it refers to the nighttime. Over the year, the first time points of the day fall within the yellow sector, the second time points of the day within the red sector and the third time points of the day within the blue sector.

Figure 3.4: The prognosis distribution of the actual Cairo Calendar prognoses was used to create random prognosis data. As 191 of the first parts of the day have good prognoses and 114 of them have bad prognoses, this ratio determined the probabilities for the first random prognosis choice of each day. The second and third random prognoses of the day were created accordingly with the ratios from real prognosis data.

structure, length and spacing of the data there is no meaningful information to be acquired by testing much shorter or longer periods.

It was also shown that standard significance estimates do not apply to the structure of the calendar, because the ratio of "good" and "bad" days would not be purely random in any case. A hemerology where all or nearly all days are "good", or nearly all "bad", would not have been likely. Thus, to simulate the real structure, we generated random prognosis data with the real ratio of "good" and "bad" prognoses in order to check the significance estimates.

We tabulated the number of good and bad prognoses over the entire calendar year.

As 191 mornings have good prognosis and 114 mornings have bad prognosis, random prognosis for the morning was created with probabilities $P(G) = \frac{191}{305}$ and $P(S) = \frac{114}{305}$. Out of the 191 good mornings, only 8 were followed by bad mid-day. Thus, the probabilities for mid-day prognosis when the morning is good were $P(GG) = \frac{183}{191}$ and $P(GS) = \frac{8}{191}$. When mid-day was also good, only 6 days in the CC had this combination followed by a bad evening. Thus, the probabilities for the evening with a good morning and good mid-day were $P(GGG) = \frac{177}{183}$ and $P(GGS) = \frac{6}{183}$. Probabilities for all other simulated prognoses were calculated accordingly and tabulated in Paper II (Fig. 3.4).

We simulated 10000 samples of aperiodic prognosis data t_i created in the aforementioned manner. The periodogram of each sample was calculated with the R-test. The median of these 10000 periodograms was the "observation noise" periodogram $z_e(f)$ that we used to estimate the reliability of standard statistics for this data. Since $z_e(f)$ showed deviation from standard Q estimates, we divided the Rayleigh test periodogram $z(f)$ of the real data with the "observation noise" $z_e(f)$. This gave us the normalized periodogram $z_N(f) = z(f)/z_e(f)$ (Paper II, Eq. 7). This normalization gave us more reliable simulated significance levels. In Paper I we used the preassigned significance level $\gamma = 0.01$ because we wanted to see if even some weak periodicity can be detected from the prognoses. However, since some of the periods reached very high significance, for the next study we used the preassigned significance level $\gamma = 0.001$ for rejecting the null hypothesis H_0 of randomness.

Earlier we had obtained three significant periods: the "lunar" period $29^{\rm d}.4$, the period $7^{\rm d}.5$ and the "Algol" period $2^{\rm d}.85$. The effect of the normalized periodogram was that the "lunar" period was shifted to $29^{\rm d}.6$ (closer to the real value of the synodic month) and an additional period $1^{\rm d}.54$ was significant in some of the samples. The effect of excluding days 1 and 20 of each month was that the "lunar" period and the $7^{\rm d}.5$ period lost their significance, but the "Algol" period became even more significant. None of the periods from the "bad" prognoses of CC reached the preassigned significance level of $\gamma = 0.001$.

The period $1^{\rm d}.54$ was a spurious period predicted by Eq. 2.11 where $P_1 = 2.85$, $P_2 = 1.0$, $k_1 = -1$ and $k_2 = 1$. The period P_2 is a predictable alias, or observation window, of the day division into morning, midday and evening. This period $1^{\rm d}.54$ was absent in samples that used the division into morning, midday and night.

3.3 Astrophysical and astronomical implications

It was noted already in Paper I that the small difference in $2^{\rm d}.85$ from the current period of Algol's variability could be evidence of changes in Algol's period. To verify this idea we needed to understand astrophysics of the mass transfer from Algol B to Algol A. The long-term increase in period is predicted by

$$\dot{P}_{\rm orb}/P_{\rm orb} = -[3\dot{m}_{\rm B}(m_{\rm A} - m_{\rm B})]/(m_{\rm A}m_{\rm B}) \tag{3.3}$$

where $\dot{P}_{\rm orb}$ is the rate of $P_{\rm orb}$ change, $m_{\rm A}$ and $m_{\rm B}$ are the masses of Algol A and B, while $\dot{m}_{\rm B}$ is the mass transfer rate[50;51]. The difference between the ancient period of Algol and current period gave $\dot{m}_{\rm B} = -2.2 \times 10^{-7} M_\odot$ per year. This is consistent with the higher mass transfer estimates[52] while other models suggest it is much lower[53]. Our research may help ascertain the previously unconfirmed rate of change in Algol's period.

The astronomical question of Paper II was: Could ancient Egyptians around 1224 BC have detected Algol's variability? I quote here these eight elimination criteria directly from the paper:

C_1: Variability fulfills $m_{\rm max} \leq 4.0$ and $\delta m \geq 0.4$.
C_2: Period is known and fulfills $1.^{\rm d}5 \leq P \leq 90^{\rm d}$.
C_3: Variable was not below, or too close to, the horizon.
C_4: Variability can be predicted.

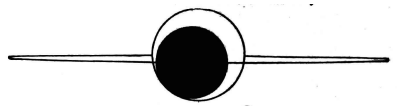

Figure 3.5: Percival Lowell's interpretation of Algol A-B system at the moment of eclipse.[54].

C_5: *Variability can be detected during a single night.*
C_6: *Variability changes the constellation pattern.*
C_7: *Period of variability could be discovered by ancient Egyptian scribes.*
C_8: *In history, which periodic variable stars were discovered first.*

Out of all 40 000 variable stars, these criteria favored Algol. Algol is the only eclipsing binary whose entire eclipse can be observed during a single night. Its variability affects noticeably the observed constellation pattern. Historically, Algol was the second detected periodic variable star.

The perturbations by Algol C on the inclination of the A-B system may change the observed eclipse over time (Fig. 3.5). Thus we needed to check that there actually were eclipses in 1224 BC. The best estimate for the angle suggests that the eclipses were similar in 1224 BC as in the present day[55].

Chapter 4

Periodicity of mythological description in the Cairo Calendar

4.1 Brightness changes and divine battles

The research question was if there are indications of such observations in the mythological texts and descriptions of CC that accompany the prognoses. For this study, we chose 28 prominent deities, nouns and locations from the text using the translations of Leitz[47] and Bakir[56]. When one of the selected words (SW) occurred in the text for a day, the date was converted into a time point which was then included in the analysis. Occurrences of SW in compound words such as Ra-Horakhti (a combination of Ra and Horus) were ignored, as were dates with an uncertain prognosis.

The time points were

$$t_i = 30(M-1) + D - 1 + m_t \tag{4.1}$$

where M is the month number and D is the day number. The constant m_t was the mean of the decimal parts from the day division in Paper II. This constant was used because usually the connection of an SW to a specific part of the day was not apparent.

The periods of Moon (P_M) and Algol (P_A) were proven significant earlier. Technically this means that phases of time points created from the prognoses, transformed to vectors r_i, are aligned instead of being randomly distributed. For example, if the sum vector $R = \sum_{i=1}^{n} r_i$ points to 0°, then all individual vectors r_i having phase angles $-90° < \theta_i < 90°$ strengthen the significance, while the remaining r_i weaken it.

In order to discover which SW strengthen or weaken the significance, we first calculated the ephemerides of the sum vectors R of the samples of series of time points (SSTP) 1, 3, 5, 7, 9 and 11 from Paper II with the periods of Moon and Algol. The ephemeris zero epoch was given by

$$t_E = t_0 + P\phi_R \tag{4.2}$$

where using zero epoch $t_0 = 0$ for the above mentioned SSTP gave $t_{E,\mathrm{Algol}} = 0.53 \pm 0.09$ and $t_{E,\mathrm{Moon}} = 3.50 \pm 0.09$. Using these ephemerides, time points with phase close to $\phi = \Theta = 0$ were considered relevant for the periodicity.

We wanted to identify which SW correlate with the Moon and Algol periodicities. All dates with an SW occurring in the text create a subset of time point series t^*.

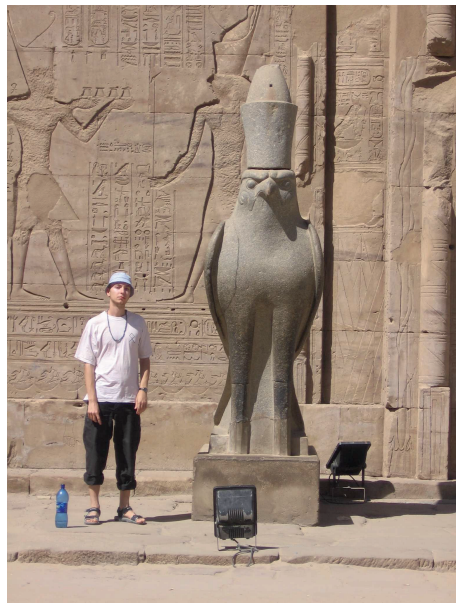

Figure 4.1: The author with a statue of Horus in front of the Temple of Edfu, 2006. Photo courtesy of Heidi Jauhiainen.

We used the ephemeris t_E in Eq. 2.1 in calculating the phases for these samples. We then computed the impact of this subset on the chosen P:

$$z_x = (R_x/|R_x|)(R_x^2/n), \tag{4.3}$$

where R_x was computed only for the n^* time points of t^*. If $z_x > 0$, the time points strengthened the periodic signal. If $z_x < 0$, they weakened the signal. We also calculated the critical level Q_z for the test statistic z_x. Our criterion for an SW being connected to a P was $z_x \geq 1.0$ and $Q_z \leq 0.2$. A more detailed explanation of the z_x and Q_z criteria is given in Paper III. We also noted the cases where t^* exhibited periodicity, but did not strengthen it (the points are not aligned with the sum vector R of the period in the sample).

For each SW, we also calculated the binomial distribution probability Q_B. It measures the presence of this particular SW in relation to all the individual vectors contributing to the sum vector R.

For each SW, the binomial distribution probability was

$$Q_B = P(n_1, n_2, N) = \sum_{i=n_1}^{n_2} \binom{n_2}{i} q_B^i (1 - q_B)^{n_2 - i}, \tag{4.4}$$

where N was the total number of prognoses N_G or N_S. Binomial probability $q_B = n_G/N_G$ or n_S/N_S was the fraction that is related to the chosen SW. Parameter n_1 was the number of vectors in this SW that are among the n_2 vectors closest to θ_R in all N_G or N_S. Thus, Q_B measures the presence of this particular SW among the vectors in the direction of θ_R.

Algol's period P_A was found to be connected to the SWs: "Horus", "Re", "Wedjat", "Followers", "Sakhmet" and "Ennead". The SWs "Heliopolis" and "Enemy" also exhibited this periodicity but did not strengthen the P_A signal. These SWs were found to be connected to Moon signal P_M: "Earth", "Heaven", "Busiris", "Rebel", "Thoth" and "Onnophris". The SW "Nut" exhibited the periodicity but did not strengthen the P_M signal.

The SW "Horus" (Fig. 4.1) had the largest impact ($z_x = +3.5$) and the highest significance ($Q_z = 0.03$) for P_A. The associated texts apparently describe Algol at its brightest (*"white crown"*, *"returned complete"*, *"entering into heaven"*). Interpretations from the phase diagram were that the good prognoses are connected with the brightest phases of Algol whereas bad prognoses occurred after Algol's eclipse (Fig. 4.2).

The SW "Sakhmet" (Fig. 4.3) was only the fifth best in order of impact ($z_x = +1.3$) on P_A but the three s_i time points in the phase diagram after the eclipse of Algol reached the lowest found binomial distribution probability: $Q_B = 0.0004$. These three unlucky prognoses are immediately followed by lucky ones. In Paper IV, we showed that they were possibly related to the myth of Destruction of Mankind where the bloodthirsty goddess Sakhmet is pacified with beer colored to look like blood.

The SW "Earth" had the largest impact ($z_x = +5.3$) and the highest significance ($Q_z = 0.001$) for the period of the Moon. Full Moon was lucky for Earth, consistent with previous knowledge regarding the ancient Egyptian lunar feasts. The SW "Heaven" also had a large impact ($z_x = +3.4$) and high significance ($Q_z = 0.03$) with P_M.

The SW "Seth" (Fig. 5.1) weakened the P_M significance (negative z_x) and thus did not strengthen the period of the Moon. But a connection of the SW to an unlucky New Moon is suggested by the descriptions of days III Peret 16-17, as already suggested by Leitz[47].

The main conclusions from the analysis of the SW were that the brightest phases of both Moon and Algol were apparently considered lucky while Algol's eclipses and the New Moon were considered unlucky. Algol was represented as a form of Horus. Seth was shown to be connected to the cycle of the Moon.

The ephemerides calculated in Paper III were used in Paper IV to study in more detail how the textual references to "Horus", "Wedjat", "Sakhmet", "Seth" and "Osiris" relate to the observed phases of Algol and Moon.

Texts referring to "Horus", "Wedjat" and "Sakhmet" were rearranged according to the phase angles Θ_{Algol}. "Horus", "Seth" and "Osiris" passages were arranged according to Θ_{Moon}. We explored how these texts correspond to the myths of "Destruction of Mankind" and "Contendings of Horus and Seth" when ordered by phase of Algol or Moon and concluded that the actions of the deities correlated with the phase at least in the bright phases of Algol and Moon.

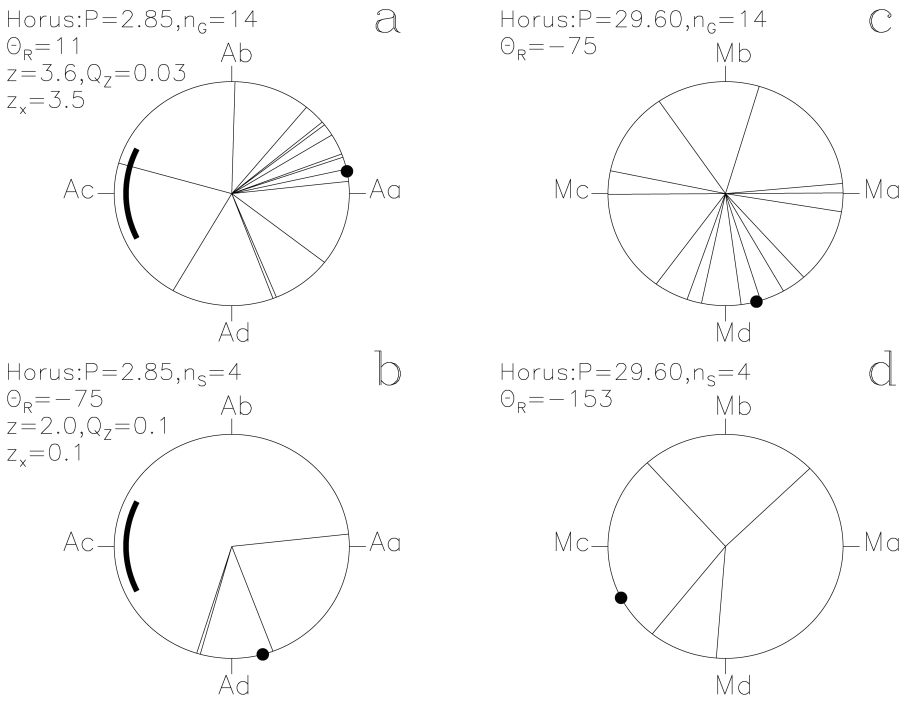

Figure 4.2: The distribution of the texts related to SW "Horus" in relation to the phases of Algol and Moon. Time runs counter-clockwise from the phase $\phi = 0$ which is the brightest phase of Algol (Aa) and Moon (Ma). The next three points Ab/Mb, Ac/Mc and Ad/Md are separated by $\delta\phi = 0.25 = 90°$. The test statistic value z, impact z_x and critical level Q_z are given where $Q_z \leq 0.2$. The concerned period is P and the number of time points in the subsample is n. The large black point indicates the direction of the sum vector Θ_R. Figure (a) shows the concentration of good prognoses in the bright phase of Algol (determined from the Q_z and z_x values, not visually). The thick line centered on point Ac ($\phi = 0.5$) outlines the 10 hour eclipse of Algol. Figure (b) shows the distribution of bad prognoses in relation to the phase of Algol. They seem to occur after Algol's eclipse. Figure (c) shows the distribution of the good prognoses of SW "Horus" in relation to the Moon and figure (d) the bad prognoses. Horus has no clear connection to P_M.

Figure 4.3: The lion goddess Sakhmet was a destructive aspect of the solar divinity. Depending on the context, she may be synonymous with Wadjet or the Eye of Horus. Drawing courtesy of Anja Isoaho.

Chapter 5

Ten arguments regarding the Cairo Calendar

We summarize the results of our study of Calendars of Lucky and Unlucky Days and the possibility of ancient Egyptians having observed the variability of Algol, in the following 10 arguments, as published in Paper IV:

Argument I: For thousands of years, the "hour-watchers" practiced the tradition of timekeeping by observing hour-stars. If Algol was not an hour-star, it certainly belonged to some hour-star pattern or related constellation.

The "hour-watchers" were scribes who observed stars in order to tell the hour of the night. These so-called star clocks are also found in funerary art[5]. Algol is the 60th brightest star in the sky[57] and could be observed in the area of the ecliptic plane, making it a suitable clock-star. We cannot reliably identify Algol from the star clocks because only a few stars have been identified with any certainty. Even if Algol wasn't actually a clock-star, its variability could easily have been noticed if the pattern around it was being observed.

Argument II: Proper timing of the nightly religious rituals relied on the fixed hour-star patterns.

In ancient Egypt, proper timing of rituals was of foremost importance[58]. At night, the Sun was considered to pass through gates, which had to be opened and their guardians appeased, helped by these rituals. Any failure by the priests in observing these rituals would run the risk of the Sun not rising the next morning. Star clocks were created to serve the purpose of measuring the beginnings and endings of the 12 night hours. Any unpredictable changes in the observed star patterns would have gained attention.

Argument III: A naked eye can easily discover the significant hour-star pattern change caused by Algol's eclipse.

Algol was prominently visible in the Egyptian night sky and any unexpected change in the observed stars would have been disturbing. Noticing Algol's variability

would have been theoretically possible for 7 hours during the eclipse and quite easy during the 3 dimmest hours of the eclipse.

Argument IV: The scribes could have discovered Algol's 2.850 = 57/20 days period from long term observations of the regular 19 and 57 days eclipse cycles.

A sequence of three night-time eclipses is repeated every 19 days in a pattern of 3+3+13 days. First, an eclipse occurs in the end of the night, three days from this first eclipse it occurs close to midnight, after the next three days again in the beginning of the night. The next observable night-time eclipse will be after 13 days. After three of these sequences complete a 57 (19+19+19) day cycle, Algol's eclipse has returned to the same hour of the night. Figure 6 in Paper IV shows how either the presence or the absence of a nightly eclipse could have been recorded by the Egyptians.

Argument V: The ancient Egyptian scribes may have calculated the 57/20 = 2.850 days period of Algol from long term observations (1st method). They may not have calculated this 2.850 days period, because the 19 days and 57 days cycles already perfectly predicted all night-time eclipses of Algol (2nd method), or they may have just recorded the observed night-time eclipses into CC (3rd method).

The ancient Babylonians and the ancient Chinese predicted the occurrence of lunar eclipses based on long-term records. The Late Egyptian papyrus Carlsberg 9 shows that Egyptians used long-term records to calculate the synodic period of the Moon. This raises the question if Algol's period could have been calculated as well (1st method). However, with the 19 and 57 day cycles mentioned in Argument IV, eclipse prediction would have been possible without a numerical estimate (2nd method). The pattern of observed eclipses could also have been transferred directly to the calendar without sophisticated advance predictions (3rd method).

Argument VI: To avoid violating cosmic order, the scribes would have referred to Algol's changes only indirectly.

As an example, solar eclipses were certainly noticed but in no ancient Egyptian written records are they mentioned directly[59]. Evidently they were considered fearsome and unlucky portents[60]. There is a high possibility that for the same reason many astronomical events like Algol's eclipses were described indirectly in mythological language by the ancient Egyptians.

Argument VII: Even a quick glance on List 1 (Paper IV) and List 2 (Paper IV) reveals that numerous CC texts are excerpts from the LE1 and LE2 legends.

List 1, in appendix C of Paper IV, includes CC texts mentioning "Horus", "Wedjat" or "Sakhmet", in order of θ_{Algol}. List 2, in appendix D of Paper IV, includes CC texts mentioning "Horus", "Seth" or "Osiris", in order of θ_{Moon}. The sequences of these texts suggest that the phases of variable astronomical objects reminded Egyptians of the actions of deities in the myths of Destruction of Mankind (LE1) and Contendings of Horus and Seth (LE2).

Figure 5.1: The god Seth, nemesis of Horus, commonly embodied disorder and rebellion. Rayleigh test of the Cairo Calendar showed a connection between Seth and the period of the Moon. Drawing courtesy of Anja Isoaho.

Argument VIII: The texts of List 1 (θ_{Algol} order) and List 2 (θ_{Moon} order) show that the LE1 and LE2 legends could have been used to describe indirectly the regular changes of Algol and the Moon.

The first principle seems to have been:

> "The middle of the bright phases of Algol and the Moon is lucky for mankind."

This is suggested by texts near Algol's brightest phase:
"the majesty of Horus receiving the white crown"
"this eye of Horus has come, is complete, is uninjured"
"Peace between Horus and Seth"
"Onnophris' happiness in giving his throne to his son Horus"
"a feast of entering into heaven, the two banks of Horus rejoice"

The times after Algol's eclipse phase were notable for negative and aggressive events involving "Horus", "Wedjat" or "Sakhmet". As for the Moon, the brightest phase seemed also the luckiest phase. The unlucky nature of the New Moon was already noted by Leitz regarding the dates III Peret 16 and 17, when one is forbidden to *"go out and see the darkness"*[47]. Also other unlucky predictions connected to Seth and Osiris were concentrated on the dark phases of the Moon. It is notable that the waxing and waning of the moon was in some Late Period sources represented as gods entering and leaving the celestial eye[61].

We tentatively proposed the second and third principles:

> "Use elements from LE1 and LE2 to indirectly describe Algol's changes (List 1)."
> "Use LE2 for indirect description of the lunar phases (List 2)."

Argument IX: Algol could have been naturally associated with Horus and called as such, because Algol can disappear and reappear.

If the Egyptians noticed Algol's variability, they would have sought to incorporate the phenomenon into their worldview of constant struggle between the forces of order and chaos[62]. For example, the eclipse might remind of the myth where Seth blinds the eye of Horus and the brightening reminds of the restoration of the eye[63]. Many different interpretations would have linked Algol's eclipse cycle to the rejuvenation of royal power and cosmic order.

Argument X: Astrophysical considerations support the idea that the 2.850 days period in CC can be the period of Algol.

The current orbital period of Algol is $2^{\mathrm{d}}.867$. The mass transfer between Algol B and Algol A could have caused the period to increase, in case the ancient Egyptian period $2^{\mathrm{d}}.850 \pm 0^{\mathrm{d}}.002$ is correct. This would agree with the predicted evolution of the Algol system[52].

We concluded that ancient Egyptians had the *means* and the *motives* for observing Algol and it is the simplest, and currently the only sensible, explanation for the $2^{\mathrm{d}}.85$ period in the prognoses of the Cairo Calendar. The period was found in only one of the three tested Calendars of Lucky and Unlucky Days which is certainly intriguing. It shows that between the different examples of calendars, there are other structural differences than some random shifts in prognoses. It is probably not useful here to speculate much about it, but the absence of the Algol period in other calendars means that is not automatically included.

Chapter 6

Periodicity in simulated crater data

6.1 Generating simulation data from probability distributions

As mentioned in section 1.2, many studies have found periodicity in the terrestrial impact crater record. The aim of Paper V was to determine the quantity and quality requirements for reliable detection of such periodicity, if it exists. We simulated crater data as would have been created by aperiodic, partly periodic or fully periodic impact events. We searched for periodicity in this simulated data and compared the chances of reliable detection with different dataset sizes and errors.

If the probability density of aperiodic impact events over time was constant, we could have used the null hypothesis H_0 for standard Rayleigh test statistics. However, erosion and other geological factors complicate the detection of older and smaller craters. The effect of erosion is apparent in actual impact crater data. From the current crater database that contained 174 impact structures, of which 89 had error estimates, two subsamples were chosen according to their age $t[Myr]$, error in age σ and diameter $D[km]$:

$$\begin{aligned} t \leq 250, \sigma \leq 20, D \geq 5 \quad (n = 33) \\ 5 \leq t \leq 300, \sigma \leq 20 \quad (n = 40) \end{aligned} \tag{6.1}$$

These subsamples were divided into ten subintervals or cycles $k = 1, ..., 10$ of equal length $(t_n - t_1)/10$. The last and oldest subintervals contain less craters than the first and newest subintervals as expected. The number of craters in subintervals k were divided by the total number of craters n to calculate the fraction of craters included in each age group. The result of dividing the craters into ten subintervals was that some subintervals included only one crater or none at all, so using this fraction as such would have been unreliable. Because of this, the average of pairs of intervals was used as shown in Table 6.1, essentially the same as we would have had only five subintervals. The sum of these fractional estimates A_k satisfied the relation $\sum_{k=1}^{K} A_k = 1$. They were used in "normalizing" the probability density function, so the detectability of newer craters in our simulations would increase as in the real data (see Fig. 1 in Paper V).

Table 6.1: Calculating the fractional estimates that were used to simulate the effect of erosion. Two subsamples of craters ($n = 33$ and $n = 40$) were divided by their age into ten subintervals k. The number of craters in each subinterval is a_1 for the first subsample and a_2 for the second subsample. Because of the small number of craters in some subintervals, more reliable fractional estimates were obtained by using the averages of two consecutive intervals as shown in columns a_3 and a_4. The average of a_3 and a_4 yielded the final fractional estimate A_k used in the simulations.

k	a_1	a_2	a_3	a_4	$A_k = (a_3 + a_4)/2$
1	4/33	3/40	6/33	7/40	0.1784
2	8/33	11/40	6/33	7/40	0.1784
3	7/33	8/40	5/33	5.5/40	0.1445
4	3/33	3/40	5/33	5.5/40	0.1445
5	3/33	6/40	3.5/33	5/40	0.1155
6	4/33	4/40	3.5/33	5/40	0.1155
7	2/33	1/40	1/33	1/40	0.0277
8	0/33	1/40	1/33	1/40	0.0277
9	1/33	1/40	1/33	1.5/40	0.0339
10	1/33	2/40	1/33	1.5/40	0.0339

The probability density and cumulative distribution functions due to the assumed effects of erosion were

$$f_2(t) = \sum_{k=1}^{K} A_k f_1(t, a_k, b_k) \tag{6.2}$$

$$F_2(t) = \sum_{k=1}^{K} A_k F_1(t, a_k, b_k), \tag{6.3}$$

where $a_k = k - 1$, $b_k = k$, $f_1(t, a_k, b_k) = \begin{cases} 0, t < a_k \\ (b_k - a_k)^{-1}, a_k \leq t < b_k \\ 0, t \geq b_k \end{cases}$

and $F_1(t, a_k, b_k) = \begin{cases} 0, t < a_k \\ (t - a_k)/(b_k - a_k)^{-1}, a_k \leq t < b_k \\ 1, t \geq b_k. \end{cases}$.

We assumed that the uncertainty in the time points is a Gaussian distribution with probability density function f_G and cumulative distribution function F_G

$$f_G(t, \mu, \sigma_P) = \frac{1}{\sigma_P \sqrt{2\pi}} \exp -\frac{1}{2}(\frac{t - \mu}{\sigma_P})^2 \tag{6.4}$$

$$F_G(t, \mu, \sigma_P) = \frac{1}{\sigma_P \sqrt{2\pi}} \int_{-\infty}^{t} \exp -\frac{1}{2}(\frac{t' - \mu}{\sigma_P})^2 \mathrm{d}t', \tag{6.5}$$

where the mean was $\mu = 0$ and σ_P was simulated error expressed in units of P σ_P values of 0.05, 0.1, 0.2 and 0.3 where simulated.

The convolution of $f_2(t)$ and $F_2(t)$ with f_G and F_G produced the aperiodic component of cratering

$$f_A(t,\sigma_P) = \sum_{k=1}^{K} A_k[F_G(t,k-1,\sigma_P) - F_G(t,k,\sigma_P)] \tag{6.6}$$

$$F_A(t,\sigma_P) = \sum_{k=1}^{K} A_k\{F_G(t,k,\sigma_P) + (t-k+1)[F_G(t,k-1,\sigma_P) - F_G(t,k,\sigma_P)] + \sigma_P^2[f_G(t,k-1,\sigma_P) - f_G(t,k,\sigma_P)]\} \tag{6.7}$$

We then simulated a series of periodic cratering events assuming $K = 10$ short comet showers happened with a period $P = 1$ at epochs $t_k = k - 1/2$, where $k = 1, 2, ..., K$. Assuming these comet showers can be estimated with a Dirac delta function at each t_k, the resulting probability density and cumulative distribution functions for the periodic component of cratering were

$$f_P(t,\sigma_P) = \sum_{k=1}^{K} A_k f_G(t,t_k,\sigma_P) \tag{6.8}$$

$$F_P(t,\sigma_P) = \sum_{k=1}^{K} A_k F_G(t,t_k,\sigma_P) \tag{6.9}$$

The sums of the periodic and aperiodic components of simulated crater data were:

$$f_{AP}(t,S,\sigma_P) = Sf_A(t,\sigma_P) + (1-S)f_P(t,\sigma_P) \tag{6.10}$$

$$F_{AP}(t,S,\sigma_P) = SF_A(t,\sigma_P) + (1-S)F_P(t,\sigma_P) \tag{6.11}$$

where the constant $0 \leq S \leq 1$ represented the ratio of the components (i.e. $S = 0$ for fully periodic and $S = 1$ for fully aperiodic impacts).

Because detectability changes over time, the null hypothesis H_0 for standard Rayleigh test statistics was not applicable. Hence, our tested hypotheses were the following four totally aperiodic hypotheses

H_1: "the cumulative distribution function for the time points t_i is $F_{AP}(t, S = 1, \sigma_P = 0.05)$".
H_2: "the cumulative distribution function for the time points t_i is $F_{AP}(t, S = 1, \sigma_P = 0.1)$".
H_3: "the cumulative distribution function for the time points t_i is $F_{AP}(t, S = 1, \sigma_P = 0.2)$".
H_4: "the cumulative distribution function for the time points t_i is $F_{AP}(t, S = 1, \sigma_P = 0.3)$".

For the same reason, we used simulated data instead of the equations of Ch. 1 to determine the critical level $P(z > z_0) < \gamma$. Simulated data was created with $n = 10, 25, 50, 75$ and 100, and with $\sigma_P = 0.05, 0.1, 0.2$ and 0.3. The simulated σ_P values are similar to those of real data, as explained in more detail in Paper V. The

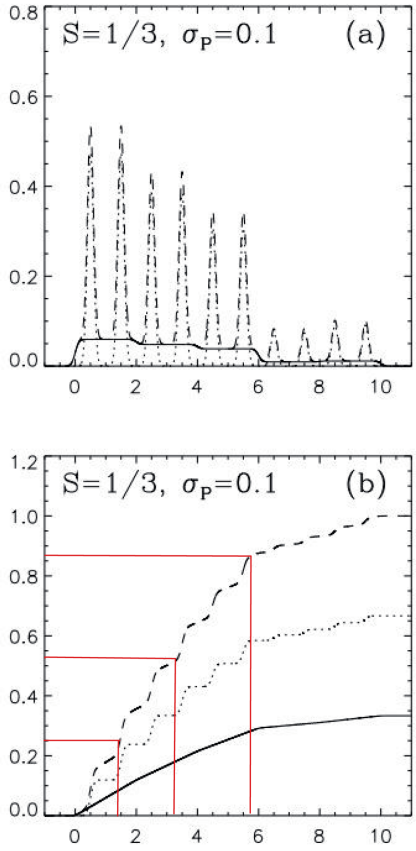

Figure 6.1: (a) Probability density function for simulated crater data with ratio of aperiodic to periodic impacts $S = 1/3$ and error expressed in units of P is $\sigma_P = 0.1$ (Eq. 6.10), where the dashed line denotes the sum of the periodic and aperiodic component, the continuous line shows only the aperiodic component and the dotted line shows only the periodic component. (b) The cumulative distribution functions for the probability density functions of (a) (Eq.6.11). Note that time (x-axis) is expressed in cycles because it does not matter what the assumed period is. The red lines show how random numbers drawn from distribution $[0, 1]$ (y-axis) yield time point values (x-axis).

time points t_i were created by drawing random numbers x_i from a uniform $[0,1]$ distribution and solving t_i in $x_i = F_{AP}(t_i, S, \sigma_P)$, using a basic inversion sampling method[64].

For each hypothesis H_1, H_2, H_3 and H_4, we created 100000 samples of aperiodic crater data using the respective probability density and cumulative distribution functions (as shown in Fig. 6.1, but using $S = 1$). For each sample, the periodogram between $0.5 \leq f \leq 2.0$ was calculated. Note that time is expressed in cycles, since the timescale is not important. The highest test statistic of each periodogram was $z_{\rm best}$. These $z_{\rm best}$ values were collected and ranked from highest to lowest. The best 1% of these $z(f_{\rm best})$ (corresponding to $\gamma = 0.01$) and the best 0.1% of these $z(f_{\rm best})$ (corresponding to $\gamma = 0.001$) determined the level of z_0 in $P(z \geq z_0) < \gamma$.

Partially periodic data ($S = 1/3$ and $S = 2/3$) and fully periodic data ($S = 0$) were simulated 100000 times for each S value using the respective probability distribution (Eqs. 6.10 and 6.11). The most significant period $P_{\rm best}$ was identified in each simulation. Note that this most significant period was not always the "real" period. The criterion for accepting the detected period as the "real" one was

$$1 - \frac{f_0}{2} \leq f_{\rm best} \leq 1 + \frac{f_0}{2}. \tag{6.12}$$

If the criterion was not fulfilled, then $P_{\rm best}$ was regarded as false.

With the z_0 value limits, it was checked if $z(f_{\rm best}) > z_0$ was true for the corresponding hypothesis $H_1, H_2, ...$ In case it was true, that hypothesis was rejected.

In addition to our aperiodic hypotheses $H_1, H_2, ...$ we tested the standard null hypothesis H_0 for sake of comparison. When $z(f_{\rm best})$ exceeded the standard critical level (Eq. 2.9), H_0 was rejected.

Fig. 2 of Paper V shows the periodogram of a sample with $S = 1/3$ and $\sigma_P = 0.1$. The vertical dotted lines depict the frequency range where the period was accepted as "real". The horizontal lines show the $\gamma = 0.01$ and $\gamma = 0.001$ levels for rejecting the hypotheses H_0 and H_2. In this sample, H_0 and H_2 were rejected at significance level $\gamma = 0.01$, but not at the $\gamma = 0.001$ level, while the detected period was accepted as a "real" one.

After all simulations for certain values of n, S and σ_P, we counted how often the period was detected. We accepted the detection as "reliable" if $H_1, H_2, ...$ was rejected with the "real" period in at least 99% (case $\gamma = 0.01$) or 99.9% (case $\gamma = 0.001$) of all Z simulations. As an example, for $S = 1/3$ and $\sigma_P = 0.1$ the period was "reliably" detected with both $\gamma = 0.01$ and $\gamma = 0.001$ and with both hypotheses H_2 and H_0 in case $n \geq 100$, since the ratio of detections vs. simulations was 1.00 or 1.000. However, for $n = 75$ and $\gamma = 0.001$ the ratio was only 0.992 (for H_2) or 0.998 (for H_0), so the periodicity detection was reliable only with $\gamma = 0.01$. Some false detections occurred with $n \leq 50$ but their probability was very small.

We also simulated rounding the ages of craters. Simulations ($Z = 100000$) of data rounded into integer multiples of $(3/\pi)\sigma_P$ were performed for all combinations of n, S and σ_P. For example, if we compare the original and rounded simulations for $S = 1/3$ and $\sigma_P = 0.1$, it can be noted that the results are slightly altered. After rounding, reliable detection was no longer possible with $\gamma = 0.01$ and $n = 50$ with hypothesis H_0, but for larger n rounding did not prevent detection.

6.2 The reliability criteria for the detection of periodicity

Our simulations revealed the necessary conditions for the reliable detection of periodicity in the impact events. If all impacts are periodic ($S = 0$), reliable detection of periodicity would be possible for most of the tested combinations if $\sigma_P \leq 0.2$. With more accurate data (lower σ_P), even small datasets ($n = 10$ or $n = 25$) would be sufficient. If only one third of the impacts were periodic ($S = 1/3$), a large dataset of $n \geq 50$ is required even with very accurate ages ($\sigma_P \leq 0.05$). With less accurate ages, even more data points are necessary for detecting the periodicity. If less than two thirds of the impacts were periodic, the possibilities to reliably detect it vanished altogether.

The main results were not substantially different when the null hypothesis H_0 was used instead of the modified hypothesis H_1, H_2, H_3 or H_4. However, H_0 was rejected more often, also in the case of "false" periods. These are evidence that the modified hypotheses were statistically more reliable. Rounding of data reduced the chances of detecting the "real" period.

The two subsets of real crater data mentioned in the beginning of this chapter can be compared to the simulations where $S = 0$ and $\sigma_P = 0.1$ or $\sigma_P = 0.2$. Reliable detection of periodicity would be possible for the first subset ($\sigma_P = 0.1$), if all impacts were periodic. The R-test for this subset was performed, but neither the hypothesis H_0 nor the above mentioned hypothesis H_2 was rejected, i.e. we did not detect periodicity. Neither was reliable detection of periodicity possible with the crater data used by Alvarez & Muller[19] or Stothers[65].

Chapter 7

Conclusions

This thesis was comprised of four papers that concerned Ancient Egyptian hemerologies and one paper where periodicity in terrestrial impact craters was explored. These different topics were unified by the Rayleigh test as a method for discovering periodicity in such "ancient" data.

In a sense, these papers overturned some expectations. Ever since Neugebauer historians of science have been sceptical regarding astronomical calculations from ancient Egypt because of lack of evidence, but our papers may have revealed an unequalled "data point" from the past. On the other hand, many well-publicized studies claimed to have discovered periodicity in the ages of terrestrial impacts, but our paper showed that it is impossible with the available data.

7.1 Algol and Moon in ancient Egypt

Ancient Egyptians utilized astronomy foremost in ritual and religious context. Lunar calendar feast dates related to the phases of the Moon played a part in Egyptian life[66;3]. It has been suggested that some well-known myths related to the observation of lunar eclipses[67]. Thus it may not come as a surprise that we found the period of the Moon in the Calendar of Lucky and Unlucky Days.

On the other hand, the influence of individual stars on Egyptian religion is an overall more mysterious matter. Only the most prominent stars and constellations such as Sirius, Orion and Big Dipper have been somewhat reliably identified but texts regarding them are disputed[68;5;69].

We established the proposed connection of Algol to Ancient Egypt by providing statistical, astronomical, astrophysical and egyptological evidence for the period $2^{\mathrm{d}}.85$ in Cairo Calendar. Provided it is true, the result has at least four consequences:
1. An actual record of the observation of a star's variability in ca. 1224 BC changes the known history of astronomy.
2. Ancient Egyptian legends and religious texts may yield new interpretations if the connection of Horus to variable stars and the luckiness of its different phases are considered.
3. If the eclipse was visible for ancient Egyptians, it constrains the orbital plane of the Algol A-B system to being nearly perpendicular to that of the Algol AB-C system.
4. The periodicity of Algol in ca. 1224 BC is a valuable constraint on calculating

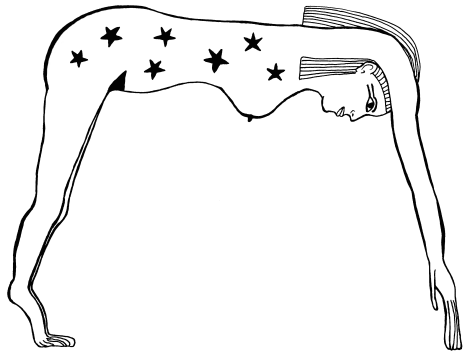

Figure 7.1: Nut, the goddess of the sky, is depicted arching over the earth. In cosmological texts, the sun and the stars are described as physically traversing through her body. Drawing courtesy of Anja Isoaho.

mass transfer in eclipsing binaries.

7.2 Terrestrial impact cratering rate

The question of periodicity in the ages of terrestrial impact craters and associated mass extinctions has understandably a multitude of voices for and against. The debate continues decades after the original discoveries of periodicity in crater data were disproven. Instead of an argument for or against a specific periodicity, our paper aimed to establish the necessary conditions for periodicity detection being at least theoretically possible. The main conclusion was that if less than two thirds of impact craters are caused by the periodic phenomena, there is no way to reliably detect the periodicity with the R-test. The ratio between periodic and aperiodic impacts is not exactly known but it would seem that aperiodic impacts dominate[70]. Moreover, the error estimates in crater ages at Earth Impact Database have in some cases increased[71]. Older craters gradually disappear due to geological processes[72] but analysis of lunar craters shows that the deficit of 250-650 Mya craters must also be due to a lower impact flux[73]. Only a small percentage of expected small impact craters has been discovered[74], but Lowe & Byerly recently proposed that the study of ejecta layers can be used to improve the terrestrial impact crater record[12]. Reliably proving periodicity in the ages of impact craters remains only a dream for now.

7.3 Rayleigh test: parting the fog of time

Regular events may seem randomly occurring over time because pieces of the puzzle are missing. Ancient texts may become undecipherable while impact craters are eroded by natural forces. The aim of these studies was to make sense of different astronomical records from the past and uncover information for our present age.

Already the first test of the Ancient Egyptian Lucky and Unlucky Days revealed significant periods in the longer series. Errors in periods were remarkably small considering the not so exact nature of the original data. In the modified test, the significance of these periods was confirmed using a noise periodogram. For the noise periodogram, we created simulated data with the structure of the original data. The modified test also improved the accuracy of the period. With corrected significance estimates the real periods of Moon and Algol became even more significant.

Simulated data was also used in estimating the possibility of periodicity detection in the terrestrial impact crater record. Detectability favours newer and larger craters, so we formulated aperiodic hypotheses to replace the null hypothesis in order to simulate the effect of erosion over time. The main results were not radically altered by the choice of hypothesis, but with the standard null hypothesis significance tended to be overestimated. Thus modified hypotheses were concluded as statistically more reliable.

Cross-disciplinary studies such as those presented here pose some additional challenges in both formulation and presentation, but if the following conclusions seem agreeable to the reader, these experiments were surely worth the effort:

1. Analysis methods of modern astronomy can benefit of historical and cultural studies.
2. Ancient Egyptian scribes' diligent observations may provide useful information to modern Astronomers.
3. Analyzing simulated time point data in addition to real time point data highly improves significance estimates of periods.

Chapter 8

Summary of the publications

This thesis consists of five peer reviewed publications:

- **Paper I:** Evidence of periodicity in ancient Egyptian calendars of lucky and unlucky days
- **Paper II:** Did the ancient Egyptians record the period of the eclipsing binary Algol - the Raging One?
- **Paper III:** Shifting milestones of natural sciences: the ancient Egyptian discovery of Algol's period confirmed
- **Paper IV:** Algol as Horus in the Cairo Calendar: the possible means and the motives of the observations
- **Paper V:** Detection of real periodicity in the terrestrial impact crater record

The papers are summarised below. The author's contribution to the papers is described at the end of each section.

8.1 Paper I

This article presents the first experiment of using the Rayleigh test to analyze the distribution of Lucky and Unlucky Days in the Ancient Egyptian hemerologies. In the hemerologies, prognoses denoting whether a day is lucky or unlucky are given for days of the year. These prognoses were tabulated from three sources: P. Cairo 86637 (the Cairo Calendar), P. BM 10474 and P. Sallier IV. For each of the three parts of the days of the year, a time point was created: one for the mid-point of the morning, one for the mid-day and one for the mid-point of the evening. Time point series were created from days that had the same prognosis combination (such as good-good-good or good-good-bad) and from day parts which had the same individual prognosis. All these series were tested using the Rayleigh test. The null hypothesis was rejected in 11 cases. It was concluded that the lucky and unlucky days were not distributed randomly but with some periodicities. The best period from the Cairo Calendar was attributed to the Moon and a less significant periodicity tentatively to Algol. The author contributed to Paper I by compiling the prognosis lists from various egyptological sources, co-planning the method of analysis, performing the analysis together with co-authors and writing the article.

8.2 Paper II

In the second article the accuracy of the Rayleigh test as given in Paper I was improved with simulated statistics obtained from simulated aperiodic prognosis data. For the real data, only the prognoses from P. Cairo 86637 were used because it was the one where the Algol period was detected. A new division of the day into three parts, where the third part represented the night instead of the evening, was tested. With the normalized periodogram, the period of the Moon shifted even closer to the actual synodic period of the Moon and the period of Algol in the Cairo Calendar was even more significant. Additional astrophysical, astronomical and egyptological evidence supported the idea of ancient Egyptians having observed Algol. It was shown that some of the current estimates of mass transfer rate from Algol B to Algol A support the possibility of the period of Algol having been $2^{\mathrm{d}}.85$ in ancient Egypt. Observation-wise, variability prediction and calculation of the periodicity would have been theoretically possible for the Egyptians. The author contributed to Paper II by compiling the data, performing the analysis together with the co-authors, verifying the astronomical and astrophysical results and co-writing the paper.

8.3 Paper III

In Cairo Calendar, texts accompanying the prognoses describe events, feasts and prohibitions for particular days. In previous articles, only the prognoses were studied while the aim of Paper III was to investigate the periodicity of selected words. From the text 28 prominent deities, nouns and locations were selected for period analysis. In this analysis only one time point for each day was used, because it was not certain which part of the day the selected word was related to. The impacts of the time points with a specific selected word on the previously discovered periods of Algol and the Moon were measured. It was concluded that the name "Horus" was connected with the period of Algol while the name "Seth" was connected with the period of the Moon. The author contributed to Paper III by gathering source data together with the co-author, translating the concerned Egyptian texts, verifying the analysis and co-writing the paper.

8.4 Paper IV

Paper IV was an egyptological background study of the proposed Algol observations. The questions were who recorded the period of Algol into the Cairo Calendar, how the variability was noticed and why it was significant for the Ancient Egyptians. The means and the motives of scribes for such observations were explained. From the selected words of Paper III, the names Horus, Wedjat, Sakhmet, Seth and Osiris were studied in more detail, in the context of two well-known ancient Egyptian myths: "Destruction of Mankind" and "Contendings of Horus and Seth". Some correspondence of the described actions of the deities with the phases of Algol and Moon was discovered. The author contributed to Paper IV by compiling the data together with the co-authors, translating the Egyptian text, formulating the analysis and co-writing the paper.

8.5 Paper V

The ages of terrestrial impact craters have been claimed to exhibit periodicity. Instead of arguing for or against a specific period, this article aimed to determine the criteria for reliable detection of any periodicity. Subsamples of real crater data provided an estimate for how erosion and other factors weaken the detectability of older craters. This estimate was used in creating simulated cratering data, with parameters for error and the ratio of periodic and aperiodic impacts. Simulated crater data samples with different accuracy and ratio of periodic versus aperiodic impacts were analyzed with the Rayleigh test. Reliable detection of periodicity in impact crater data was shown to be currently impossible, unless most or all of the impacts would have been periodic. The author contributed to Paper V by verifying the data and analysis, and assisting in writing the paper.

Chapter 9

Glossary

CC	The Cairo Calendar
decan	A star or star group named in the Ancient Egyptian star clocks
hemerology	A calendar of lucky and unlucky days
prognosis (G / S)	Evaluation if a day is G, "good", or S, "bad"
R-test	Rayleigh test
SSTP	Samples from series of time points
SW	Selected words from the Cairo Calendar

Bibliography

[1] N. Lockyer. *The Dawn of Astronomy: A Study of the Temple-worship and Mythology of the Ancient Egyptians*. Macmillan, 1894.

[2] Rolf Krauss. *Egyptian Calendars and Astronomy*, volume 1 of *The Cambridge History of Science*, page 131–143. Cambridge University Press, 2018.

[3] R. A. Parker. Ancient egyptian astronomy. *Philosophical Transactions of the Royal Society of London. Series A, Mathematical and Physical Sciences*, 276 (1257):51–65, 1974. ISSN 00804614.

[4] Wikimedia Commons. The double wall mural of the tomb of senenmut, 2010. URL `https://commons.wikimedia.org/wiki/File:Senenmut.jpg`. File: Senenmut.jpg.

[5] M. Clagett. *Ancient Egyptian Science, Vol 2: Calendars, Clocks and Astronomy*. American Philosophical Society, Philadephia, USA, 1995.

[6] O. Neugebauer and R.A. Parker. *Egyptian Astronomical Texts I*. Brown Univ. Press, London, England, 1960.

[7] B. Porter and R. L. Moss. *Topographical bibliography of ancient Egyptian hieroglyphic texts, reliefs and paintings*, volume 1. Clarendon Press, Oxford, UK, 1927.

[8] A. Lieven. *Grundriß des Laufes der Sterne: Das sogenannte Nutbuch*. Carsten Niebuhr Institute Publications, Museum Tusculanum Press, Copenhagen, Denmark, 2007.

[9] Daniela Comelli, Massimo D'orazio, Luigi Folco, Mahmud El-Halwagy, Tommaso Frizzi, Roberto Alberti, Valentina Capogrosso, Abdelrazek Elnaggar, Hala Hassan, Austin Nevin, Franco Porcelli, Mohamed G. Rashed, and Gianluca Valentini. The meteoritic origin of tutankhamun's iron dagger blade. *Meteoritics & Planetary Science*, 51(7):1301–1309, 2016.

[10] R.J. Huggett. *The Natural History of Earth: Debating Long-Term Change in the Geosphere and Biosphere*. Routledge Studies in Physical Geography and Environment. Taylor & Francis, 2006. ISBN 9781134246434.

[11] D. Steel. Impacts and mass extinctions: To whom the laurel falls? *Journal of the British Astronomical Association*, 104:292–292, December 1994.

[12] Donald R. Lowe and Gary R. Byerly. The terrestrial record of Late Heavy Bombardment. *New Astronomy Review*, 81:39–61, Apr 2018.

[13] Wikimedia Commons. File:gosses bluff crater 1984 7s41000400889.jpg — wikimedia commons, the free media repository, 2019. URL `https://commons.wikimedia.org/w/index.php?title=File:Gosses_Bluff_crater_1984_7S41000400889.jpg&oldid=350180799`. [Online; accessed 2-November-2019].

[14] H. C. Urey. Cometary Collisions and Geological Periods. *Nature*, 242:32–33, March 1973.

[15] C. J. Sprain, P. R. Renne, W. A. Clemens, G. P. Wilson, S. M. Smith, D. L. Lofgren, S. Self, L. Vanderkluysen, K. Pande, and T. Mittal. Timescale of Events Around the Cretaceous-Paleogene Boundary: Links Between the Chicxulub Impact, Deccan Volcanism, and the Cretaceous-Paleogene Boundary. In *AGU Fall Meeting Abstracts*, volume 2018, pages PP54B–01, Dec 2018.

[16] Christian Koeberl. When Earth got pummeled. *Science*, 363:224–225, Jan 2019.

[17] F. Feng. *Investigations into the impact of astronomical phenomena on the terrestrial biosphere and climate*. PhD thesis, Heidelberg University, Jan 2016.

[18] D. M. Raup and J. J. Sepkoski. Periodicity of Extinctions in the Geologic Past. *Proceedings of the National Academy of Science*, 81:801–805, February 1984.

[19] W. Alvarez and R. A. Muller. Evidence from crater ages for periodic impacts on the earth. *Nature*, 308:718–720, April 1984.

[20] M. R. Rampino and R. B. Stothers. Terrestrial mass extinctions, cometary impacts and the sun's motion perpendicular to the galactic plane. *Nature*, 308: 709–712, April 1984.

[21] R. D. Schwartz and P. B. James. Periodic mass extinctions and the sun's oscillation about the galactic plane. *Nature*, 308:712, April 1984.

[22] D. P. Whitmire and A. A. Jackson. Are periodic mass extinctions driven by a distant solar companion? *Nature*, 308:713–715, April 1984.

[23] M. Davis, P. Hut, and R. A. Muller. Extinction of species by periodic comet showers. *Nature*, 308:715–717, April 1984.

[24] Michael P Gillman, Hilary E Erenler, and Phil J Sutton. Mapping the location of terrestrial impacts and extinctions onto the spiral arm structure of the milky way. *International Journal of Astrobiology*, 18(4):323–328, 2019.

[25] R. A. Rohde and R. A. Muller. Cycles in fossil diversity. *Nature*, 434:208–210, March 2005.

[26] Adrian L. Melott and Richard K. Bambach. A ubiquitous 62-myr periodic fluctuation superimposed on general trends in fossil biodiversity. i. documentation. *Paleobiology*, 37(1):92–112, 2011. doi: 10.1666/09054.1.

[27] Michael R. Rampino and Ken Caldeira. Periodic impact cratering and extinction events over the last 260 million years. *Monthly Notices of the RAS*, 454:3480–3484, Dec 2015.

[28] Matthias M. M. Meier and Sanna Holm-Alwmark. A tale of clusters: no resolvable periodicity in the terrestrial impact cratering record. *Monthly Notices of the RAS*, 467:2545–2551, May 2017.

[29] F. Feng and C. A. L. Bailer-Jones. Assessing the Influence of the Solar Orbit on Terrestrial Biodiversity. *The Astrophysical Journal*, 768:152, May 2013.

[30] C. A. L. Bailer-Jones. Bayesian time series analysis of terrestrial impact cratering. *Monthly Notices of the Royal Astronomical Society*, 416:1163–1180, September 2011.

[31] J. T. Wickramasinghe and W. M. Napier. Impact cratering and the Oort Cloud. *Monthly Notices of the Royal Astronomical Society*, 387:153–157, June 2008.

[32] Heon-Young Chang and Hong-Kyu Moon. Time-Series Analysis of Terrestrial Impact Crater Records. *Publications of the Astronomical Society of Japan*, 57 (3):487–495, June 2005. ISSN 0004-6264.

[33] L. Jetsu and J. Pelt. Spurious periods in the terrestrial impact crater record. *Astronomy & Astrophysics*, 353:409–418, January 2000.

[34] James R. Beniger and Dorothy L. Robyn. Quantitative graphics in statistics: A brief history. *The American Statistician*, 32(1):1–11, 1978. ISSN 00031305.

[35] E. Batschelet. *Circular Statistics in Biology*. Mathematics in biology. Academic Press, 1981. ISBN 9780120810505.

[36] C. M. Jackman, C. Knigge, D. Altamirano, R. Gladstone, W. Dunn, R. Elsner, R. Kraft, G. Branduardi-Raymont, and P. Ford. Assessing quasi-periodicities in jovian x-ray emissions: Techniques and heritage survey. *Journal of Geophysical Research: Space Physics*, 123(11):9204–9221, 2018.

[37] L. Jetsu, T. Hackman, D. S. Hall, G. W. Henry, M. Kokko, and J. You. Time series analysis of V815 Herculis photometry between 1984 and 1998. *Astronomy & Astrophysics*, 362:223–235, October 2000.

[38] K. T. S. Brazier. Confidence intervals from the Rayleigh test. *Monthly Notices of the Royal Astronomical Society*, 268(3):709–712, 06 1994. ISSN 0035-8711.

[39] K. Pearson. The Problem of the Random Walk. *Nature*, 72:342, August 1905. doi: 10.1038/072342a0.

[40] M.N. Barber, B.W. Ninham, and B.W. Ninham. *Random and Restricted Walks: Theory and Applications*. Mathematics and its aplications : A series of monographs and texts. Gordon and Breach, 1970. ISBN 9780677026206.

[41] J. D. Scargle. Studies in astronomical time series analysis. II. Statistical aspects of spectral analysis of unevenly spaced data. *The Astrophysical Journal*, 263: 835–853, December 1982. doi: 10.1086/160554.

[42] T. J. Deeming. Fourier Analysis with Unequally-Spaced Data. *Astrophysics & Space Science*, 36(1):137–158, August 1975.

[43] Rayleigh. The Problem of the Random Walk. *Nature*, 72:318, August 1905.

[44] B. Efron and R. Tibshirani. Bootstrap methods for standard errors, confidence intervals, and other measures of statistical accuracy. *Statist. Sci.*, 1(1):54–75, 02 1986.

[45] W. Wreszinski. Tagewählerei im alten Ägypten. *Archiv für Religionwissenschaft*, 16:86–100, 1913.

[46] E. Brunner-Traut. Mythos im Alltag. *Antaios*, 12:332–347, 1970.

[47] C. Leitz. *Tagewählerei. Das Buch und verw andte Texte.* Harrassowitz, Wiesbaden, Germany, 1994.

[48] Rolf Krauss. The Eye of Horus and the Planet Venus: Astronomical and Mythological References. *Altes Orient und Altes Testament*, 297, 2002.

[49] Wikimedia Commons. File:gallery of antiquities, selected from the british museum (1842) (14776748924).jpg — wikimedia commons, the free media repository, 2019. URL `https://commons.wikimedia.org/w/index.php?title=File:Gallery_of_antiquities,_selected_from_the_British_Museum_(1842)_(14776748924).jpg&oldid=343588459`. [Online; accessed 3-November-2019].

[50] A. Erdem and O. Öztürk. Non-conservative mass transfers in Algols. *Monthly Notices of the Royal Astronomical Society*, 441(2):1166–1176, 05 2014. ISSN 0035-8711.

[51] K. K. Kwee. Investigation of variations in the period of sixteen bright short-period eclipsing binary stars. *Bulletin of the Astronomical Institute of the Netherlands*, 14:131, April 1958.

[52] M. J. Sarna. The evolutionary status of Beta Per. *Monthly Notices of the Royal Astronomical Society*, 262:534–542, May 1993.

[53] Kristen Wecht. *Determination of mass loss and mass transfer rates of Algol (Beta Persei) from the analysis of absorption lines in the UV spectra obtained by the IUE satellite.* PhD thesis, Lehigh University, January 2006.

[54] Wikimedia Commons. File:the evolution of worlds 0024-t.jpg — wikimedia commons, the free media repository, 2017. URL `https://commons.wikimedia.org/w/index.php?title=File:The_Evolution_of_Worlds_0024-T.jpg&oldid=245988033`. [Online; accessed 3-November-2019].

[55] F. Baron, J. D. Monnier, E. Pedretti, M. Zhao, G. Schaefer, R. Parks, X. Che, N. Thureau, T. A. ten Brummelaar, H. A. McAlister, S. T. Ridgway, C. Farrington, J. Sturmann, L. Sturmann, and N. Turner. Imaging the Algol Triple System in the H Band with the CHARA Interferometer. *The Astrophysical Journal*, 752:20, June 2012.

[56] A. Bakir. *The Cairo Calendar No. 86637.* Government Printing Office, Cairo, Egypt, 1966.

[57] D. Hoffleit and C. Jaschek. *The Bright star catalogue*. Yale University, USA, 1991.

[58] J. Assmann and D. Lorton. *The Search for God in Ancient Egypt*. Cornell University Press, New York, USA, 2001.

[59] D. G. Smith. Solar Eclipse Events in the New Kingdom. Part 2 - Astronomical Analysis. *Egyptological Journal, Articles*, 6, October 2012.

[60] A von Lieven. Divination in Ägypten. *Altorientalische Forschungen*, 26:77–120, 1999.

[61] A. von Lieven. *Der Himmel Über Esna: Eine Fallstudie Zur Relgiösen Astronomie in Ägypten Am Beispiel Der Kosmologischen Decken - Und Archtravinschriften Im Tempel Von Esna* . Harrassowitz, Weisbaden, Germany, 2000.

[62] G. Magli. *Architecture, Astronomy and Sacred Landscape in Ancient Egypt*. Cambridge University Press, Cambridge, UK, 2013.

[63] J.P. Allen. *The Ancient Egyptian Pyramid Texts*. Society of Biblical Literature, Leiden, The Netherlands, ed. Der Manuelian, P., 2005.

[64] Luca Martino, David Luengo, and Joaquín Míguez. *Direct Methods*, pages 27–63. Springer International Publishing, Cham, 2018.

[65] R. B. Stothers. The period dichotomy in terrestrial impact crater ages. *Mon. Not. Roy. Astron. Soc.*, 365:178–180, 2006.

[66] R. A Wells. *"Re and the Calendars", in Revolution in Time: Studies in Ancient Egyptian Calendrics*. Van Siclen Books, San Antonio, USA, 1994.

[67] J. Sellers. *The Death of Gods in Ancient Egypt*. Lulu.com, 2007. ISBN 9781430317906.

[68] R. Krauss. *Stellar and solar components in ancient Egyptian mythology and royal ideology*. British Archaeological Reports, eds. M.A. Rappenglück, B. Rappenglück, N. Campion and F. Silva, Oxford, England, 2016.

[69] Rolf Krauss and V. Reijs. Babylonian Crescent Observation and Ptolemaic-Roman Lunar Dates. *Palarch's Journal of Archaeology of Egypt/Egyptology*, 9: 1–95, 2012.

[70] W. F. Bottke, A. Morbidelli, R. Jedicke, J.-M. Petit, H. F. Levison, P. Michel, and T. S. Metcalfe. Debiased Orbital and Absolute Magnitude Distribution of the Near-Earth Objects. *Icarus*, 156:399–433, April 2002.

[71] Earth impact database, Accessed March 22, 2020. URL `http://www.passc.net/EarthImpactDatabase/Newwebsite_05-2018/Index.html`.

[72] V. A. Zaitsev. Model of Terrestrial Impact Craters Preservation. *LPI Contributions*, 2067:6298, Jul 2018.

[73] W. F. Bottke, S. Mazrouei, R. R. Ghent, A. H. Parker, and T. M. Gernon. What Really Happened to Earth's Older Craters? In *Lunar and Planetary Science Conference*, page 1457, Mar 2018.

[74] T. Platz, G. G. Michael, O. Hartmann, and T. Kenkmann. Earth's Expected Impact Crater Record on Regional and Global Scales. In *Lunar and Planetary Science Conference*, page 2838, Mar 2013.